DESIGN AND ANALYSIS OF A FLAPPING WING OF A MICRO AERIAL VEHICLE USING IONIC POLYMER METAL COMPOSITE

RAMAIAH
Institute of Technology

A PROJECT REPORT SUBMITTED TO

RAMAIAH INSTITUTE OF TECHNOLOGY, BANGALORE.

In partial fulfillment of the requirements for the award of the degree of

BACHELOR OF ENGINEERING
in
MECHANICAL ENGINEERING

By

ABHIRAM BHARADWAJ	**1MS13ME003**
ABISHEK BHAT B R	**1MS13ME006**
GAURAV A A	**1MS13ME053**
K LEELA SAI PRABHAT REDDY	**1MS13ME067**

Under the guidance of

Internal Guide

Dr. C. M. RAMESHA
Associate Professor,
Department of Mechanical Engineering
Ramaiah Institute of Technology, Bangalore.

External Guide

Dr. DINESHKUMAR HARURSAMPATH
Professor,
Department of Aerospace Engineering
Indian Institute of Science, Bangalore.

DEPARTMENT OF MECHANICAL ENGINEERING
RAMAIAH INSTITUTE OF TECHNOLOGY
(Autonomous Institute, Affiliated to VTU)
Bangalore – 560054

May 2017

DEPARTMENT OF MECHANICAL ENGINEERING

RAMAIAH INSTITUTE OF TECHNOLOGY
(Autonomous Institute, Affiliated to VTU)
Bangalore – 560054.

Project Report 2016 – 2017

CERTIFICATE

This is to certify that the following students who are working under our guidance, have completed their work as per our satisfaction with the topic "**DESIGN AND ANALYSIS OF A FLAPPING WING OF A MICRO AERIAL VEHICLE USING IONIC POLYMER METAL COMPOSITE**". To the best of our understanding, the work to be submitted in this report does not contain any work which has been previously carried out by others and submitted by the candidates for themselves for the award of any degree anywhere.

Dr. C. M. Ramesha	**Dr. D. Ramesh Rao**	**Dr. N. V. R. Naidu**
Associate Professor Department of Mechanical Engineering, RIT.	Head of the Department Department of Mechanical Engineering, RIT.	Principal Ramaiah Institute of Technology

External Examiners

1.

2.

DEPARTMENT OF MECHANICAL ENGINEERING

RAMAIAH INSTITUTE OF TECHNOLOGY
(Autonomous Institute, Affiliated to VTU)
Bangalore – 560054.

Project Report 2016 – 2017

DECLARATION

We hereby declare that the entire work embodied in this project has been carried out by us at **Indian Institute of Science** under the guidance of **Dr. Dineshkumar Harursampath, Professor, Aerospace Engineering Department** and our internal guide **Dr. C. M. Ramesha, Department of Mechanical Engineering**, **Ramaiah Institute of Technology.** This report has not been submitted in part or full for the award of any diploma or degree of this or any other university.

ABHIRAM BHARADWAJ
(1MS13ME003)

ABISHEK BHAT B R
(1MS13ME006)

GAURAV A A
(1MS13ME053)

K LEELA SAI PRABHAT REDDY
(1MS13ME067)

Design and Analysis of a Flapping Wing of a Micro Aerial Vehicle using Ionic Polymer Metal Composite

May 24, 2017

Acknowledgements

Successful completion of any project in any sphere of life requires co-operation, support, guidance and inspiration from various quarters. We would like to avail this opportunity to express our sincere thanks and gratitude to all of them who have helped us, guided and supported us in our endeavor.

First of all, we would like to express our profound gratitude to our beloved Principal, **Dr. N. V. R. Naidu**, and **Dr. D Ramesh Rao**, Head of the Department of Mechanical Engineering, Ramaiah Institute of Technology, Bangalore for inspiring and motivating us to bring out a successful project.

We are sincerely grateful to our guide and mentor, **Dr. C M Ramesha**, Associate Professor, Department of Mechanical Engineering, Ramaiah Institute of Technology whose guidance, co-operation and encouragement helped us in nurturing our project.

We would like to thank **Dr. Dineshkumar Harursampath**, Professor, Department of Aerospace Engineering, Indian Institute of Science, Bangalore for giving us this wonderful opportunity and facility to carry out this project in a world renowned esteemed institution without whose expertise this project would not have been possible.

We are greatly indebted to **Smt. Srikumari Mam**, whose assistance at every stage guided our project in the right direction without which our project would have been a rudderless ship.

We would like to extend our gratitude and acknowledge the support of our **parents and friends** for their immense love and extended support in numerous ways.

Abstract

A Micro Aerial Vehicle (MAV) is a class of Unmanned Air Vehicles (UAVs). According to Defence Advanced Research Project Agency (DARPA), an MAV is defined by size as any aerial vehicle that measures less than 6 inch (15 cm) and 4-ounce weight.

Ionic polymer–metal composites (IPMCs) are synthetic composite nanomaterials, typically consisting of a polyelectrolyte membrane (usually Nafion or Flemion) plated on both faces by a noble metal such as Platinum or Gold, that display artificial muscle behavior under an applied voltage or electric field. Strips of these composites can undergo large bending and flapping displacement if an electric field is imposed across their thickness.

IPMCs have many advantages over materials that are functionally similar, such as piezo-composites, including large bending actuation, low weight, low power consumption, and flexibility. These advantages coincide with the requirements of flapping-wing motion in flapping-wing micro-aerial vehicle (FW-MAV). Thus, IPMCs can be used as actuators for the generation of flapping-wing motions.

We intend to design and analyze flapping wing model actuated by IPMC strip and come up with the optimal design. The structure of the flapping wing was modelled from insect flight aerodynamics as a biomimetic inspiration (based on previous research work) and subjected to finite element analysis for a safe design. The design and analysis of the IPMC strip was carried out in a Multiphysics software to obtain the suitable displacements, force and operating parameters. Optimizations of these parameters in the softwares was carried out by the investigation of range of values of operating parameters and choosing the most suitable combination of those to achieve the optimum flight characteristics of the micro aerial vehicle.

Such flapping-wing MAVs can be used to understand insect flight and to provide practical uses, such as flying through cracks in concrete to search for earthquake victims or exploring radioactivity-contaminated buildings, reconnaissance, surveillance, defence applications, weather forecast, traffic monitoring, biochemical sensing, inspection of pipes etc.

Keywords: Flapping Wing, Micro Aerial Vehicle, IPMC.

Contents

1 Introduction **7**

1.1 Micro Aerial Vehicles (MAVs) 7

1.1.1 Advantages of MAVs 10

1.1.2 Disadvantages of MAVs 11

1.2 Ionic Polymer Metal Composites (IPMCs) 11

1.2.1 Properties of IPMCs that make it ideal for use in Flapping Wing Micro Aerial Vehicles 14

2 Literature Survey **15**

2.1 Flapping Wing MAVs 15

2.1.1 Applications of MAVs 16

2.2 A deeper understanding of IPMCs 17

2.2.1 Manufacturing and Synthesis 17

2.2.2 Chemical Plating Methods 18

2.2.3 Mechanical Plating Methods 20

2.2.4 Microstrucure 21

2.2.5 Actuation Mechanism 22

2.2.6 Properties and Characterization of IPMCs 23

2.2.6.1 Polymer Properties 23

2.2.6.2 Ion-Exchange Capacity 24

2.2.6.3 Solvent Content and Swelling 24

2.2.6.4 Ion Migration Rates 24

2.2.6.5 Metal Content and Distribution 25

2.2.6.6 Stiffness . . . 25
2.2.7 Advantages / Disadvantages of IPMCs . . . 25
2.2.8 Application of IPMCs in Flapping Wing MAVs and other Bio-mimetic Robots . . . 26
2.2.8.1 Bio-mimetic Robotic Fish [4] . . . 26
2.2.8.2 A Bio-mimetic Jellyfish Robot [33] . . . 27
2.2.8.3 Tadpole robot [21] . . . 27
2.2.8.4 Flapping Wing MAV using IPMC [10] . . . 27

3 Aim and Scope of Present Work 30
3.1 Aim of Present Work . . . 30
3.2 Approach of Present Work . . . 31
3.3 Scope of Work . . . 32

4 Research Methodology 33
4.1 Design . . . 33
4.2 Electrochemical Analysis . . . 34
4.2.1 Ionic Model . . . 34
4.2.2 Mechanics Model . . . 35
4.3 Modelling in COMSOL . . . 37
4.3.1 Pre-Processor . . . 37
4.3.1.1 Geometries . . . 38
4.3.1.2 Meshing . . . 41
4.3.1.3 Physics . . . 44
4.3.2 Solver . . . 45
4.3.3 Post Processing . . . 45

5 Results and Conclusion 46
5.1 Ionic Transport Model . . . 46
5.2 Solid Mechanics Model . . . 49
5.3 Discussions/Conclusions . . . 61

6 Scope for Future Work 62

List of Figures

1.1 Micro STAR (Fixed Wing) 8

1.2 Micro Craft iSTAR (Rotary Wing) 9

1.3 Microbat (Flapping Wing) 10

1.4 Illsutration to show the ions, water and polymer chain inside an IPMC, along with an SEM image of the cross-section when no external input is exerted (a); the electromechanical effect in an IPMC causing the IPMC to bend, with a photograph showing the IPMC bending under electric field (b); and the mechanoelectrical effect due to charge motion on mechanical bending (c) [24]. 13

2.1 IPMC schematics indicating surface morphology, interface, and cluster structure. 21

2.2 Operating principle of IPMC as actuator [13] 23

2.3 Fundamental of IPMC as a motion sensor [13] 23

2.4 Schematic diagram of the flapping actuator module developed using IPMC.[10] 28

2.5 Picture of the flapping actuator module[10] 28

4.1 Dragonfly Wing 33

4.2 Basic Wing Structure 34

4.3 IPMC Strip initially modelled in 3D 39

4.4 IPMC Strip Zoomed in 39

4.5 The Final 2D Geometry 40

4.6 2D Final Geometry zoomed in 40

4.7 Finalized Wing Geometry for Mechanical Analysis 41

4.8 Mesh for Ionic Transport Model 42

4.9 Mesh for Ionic Transport Mode - Closer Look 42
4.10 2D Mesh 43
4.11 2D mesh Zoomed in 43
4.12 Mesh used for the Solid Mechanics Model 44

5.1 Voltage distribution within the membrane, ϕ 46
5.2 Cation Concentration within the polymer 47
5.3 Cation concentration zoomed in 47
5.4 Cation concentration along the cross-section 48
5.5 Average Cation Concentration at Upper Boundary 48
5.6 Average Cation Concentration at Lower Boundary 49
5.7 Complete flapping cycle 50
5.8 6.5 mm Overlap 51
5.9 4.5 mm Overlap 51
5.10 2.5 mm Overlap 52
5.11 Wing Tip Displacement for 6.5 mm Overlap 52
5.12 Wing Tip Displacement for 4.5 mm Overlap 53
5.13 Wing Tip Displacement for 2.5 mm Overlap 53
5.14 Von Mises Stresses for 6.5 mm Overlap 54
5.15 Von Mises Stresses for 4.5 mm Overlap 55
5.16 Von Mises Stresses for 2.5 mm Overlap 56
5.17 Wing Tip Displacement for 5mm thick IPMC and 2.5 mm Overlap 57
5.18 Von Mises Stresses for 5mm thick IPMC and 2.5 mm Overlap 58
5.19 Tip Displacement for 5 Hz Input and 6.5mm overlap 59
5.20 Von Mises Stresses for 5 Hz input and 6.5 mm overlap 60

Chapter 1

Introduction

1.1 Micro Aerial Vehicles (MAVs)

Micro Aerial Vehicles (MAVs) is a class of Un-manned Aerial Vehicles (UMAVs) that has size restrictions and is autonomous. According to Defense Advanced Research Project Agency (DARPA), a MAV is defined as less than 15 cm and ~115 g weight. It is semi autonomous, can be used for remote observation of hazardous environments. Lift for flight can be generated by fixed wings, rotary wings or flapping wings. The following figures show MAVs having different methods of lift generation.

Micro Air Vehicles are a class of UAVs whose time has just about come. A confluence of key events is about to occur that will enable these versatile aircraft to have military effects disproportionate to their diminutive size. The supporting technologies are progressing rapidly to the point that first simple, short-duration missions will be possible, then with time, more varied and enduring applications. At the same time, the need for weapons that help achieve the Joint Chief of Staff vision for dominant manoeuvring precision engagement, full dimensional protection, and focused logistics will be more pressing than ever. The military utility of MAVs in this context can only grow as they come closer to realizing their potential. At the start, MAVs could find application by providing localized imaging reconnaissance. Then as other key technologies mature, uses may expand to electronic warfare, nuclear, biological, and chemical agent warning, and battle damage assessment. Later still, we could see MAVs autonomously flying through airshafts reconnoitring deeply buried bunkers and reporting back to enable proper configuration of penetrating weapons.

Figure 1.1: Micro STAR (Fixed Wing)

Figure 1.2: Micro Craft iSTAR (Rotary Wing)

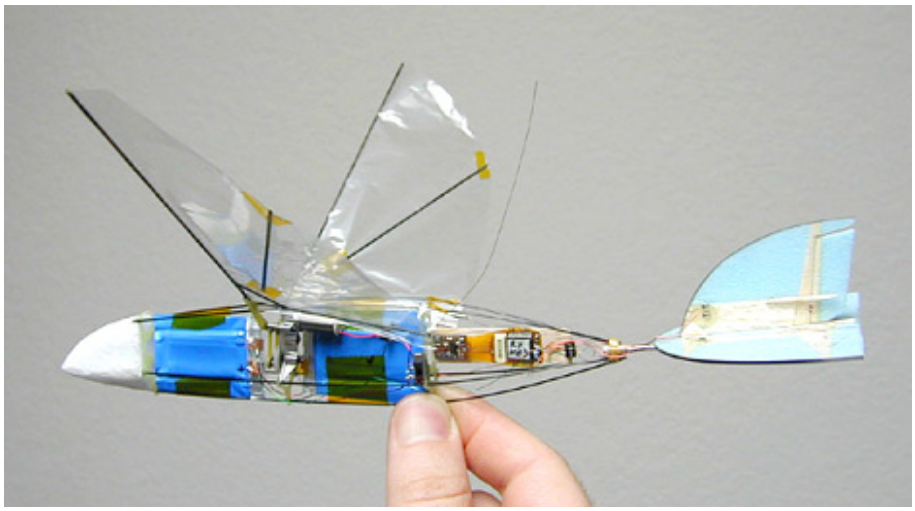

Figure 1.3: Microbat (Flapping Wing)

1.1.1 Advantages of MAVs

There are several advantages of MAVs:

- Small size and light weight
- Low power requirements
- High reusability
- Speed is 10-15 m/sec, this is not detected by most present-day radars
- High stability and control
- High lift and slow landing speed
- Can be individually controlled

1.1.2 Disadvantages of MAVs

There are several disadvantages of MAVs:

- Low image quality due to blurring
- Small range of communication
- Very difficult to design flapping wing mechanism
- Very difficult to control MAVs in bad weather
- Very expensive to design MAVs
- Lithium batteries are expensive compared to the common alkaline batteries

1.2 Ionic Polymer Metal Composites (IPMCs)

Any material that responds to external stimuli in real time is referred to as a 'smart' material. Based on their responses to an external stimulus, smart materials are classified as 'property changing' or 'energy exchanging'. In the case of 'property changing' materials the input energy causes a chemical, mechanical, thermal or electrical change in material properties. On the other hand, 'energy exchanging' materials respond with changes in their internal energy level while their material properties remain the same. The response of the materials in either category is reversible and direct [29].

From the large variety of materials, electroactive polymers (EAPs) have received a significant amount of attention due to their inherent advantages such as their low weight, flexibility, fracture tolerance and ability to take on shapes. EAPs are typically classified as 'electronic' or 'ionic', based on their specific operating principle. The actuation in electronic EAPs (eEAPs) is driven by the electrostatic mechanism due to the presence of dipoles. On the other hand, ionic EAPs (iEAPs) actuate due to the diffusion or transport of ions within the polymer membrane. While eEAPs can hold induced displacement under DC activation, iEAPs require an electrolyte for actuation. However, due to their bi-directional actuation and low voltage requirements iEAPs are being considered for biomedical, space exploration, robotics and naval applications[29].

Ionic polymer metal composites (IPMCs), which are iEAPs, are capable of electromechanical and mechanoelectrical response to applied voltage and mechanical deformation, respectively. A typical IPMC consists of a thin (200 μm) polymer membrane with metal electrodes (5–10-μm thick) plated on both faces. The polymer membrane allows selective ions to pass

through while blocking others. Since the cations are cross-linked to polymer chains, in the dry state, they are not free to move. However, on hydration, water molecules surround the cations; this makes the entire entity mobile.[29]

A cross-sectional scanning electron microscope (SEM) image of an IPMC is shown in Figure-1.4. The polymer membrane allows selective ions to pass through while blocking others. Since the cations are cross-linked to polymer chains, in the dry state, they are not free to move. However, on hydration, water molecules surround the cations; this makes the entire entity mobile. The electromechanical transduction occurs due to the motion of the cations toward the cathode (cation-rich layer), along with water molecules, on application of an electric field (figure 1(c)). This causes the IPMC to swell near the cathode. The strain in the cation-rich layer induces extensional stresses in the polymer, resulting in a fast bending motion toward the anode (cation-poor layer) [18]. The pressure from the strained polymer matrix causes water to diffuse out of the cation-rich areas, resulting in a slow relaxation toward the cathode. A bending response under the influence of a low voltage of about 1–2 V of an IPMC was first reported by Oguro et al [20], and Shahinpoor et al [26] also reported similar findings at the same time.

Currently, the application of IPMCs is limited to the research environment due to their inherent short comings such as non-linear response, low force output during actuation and low current output during sensing. The transduction in IPMCs has been observed to be dependent on the polymer layer properties (type of polymer, counter ion, conductivity and the degree of hydration), the electrode layer properties (type, area and thickness) and the intermediate layer properties (area and thickness). An understanding of these layers and their properties is vital for improving their transduction capabilities and the viability of IPMC applications. The most important among these capabilities are transducer authority and transduction efficiency.

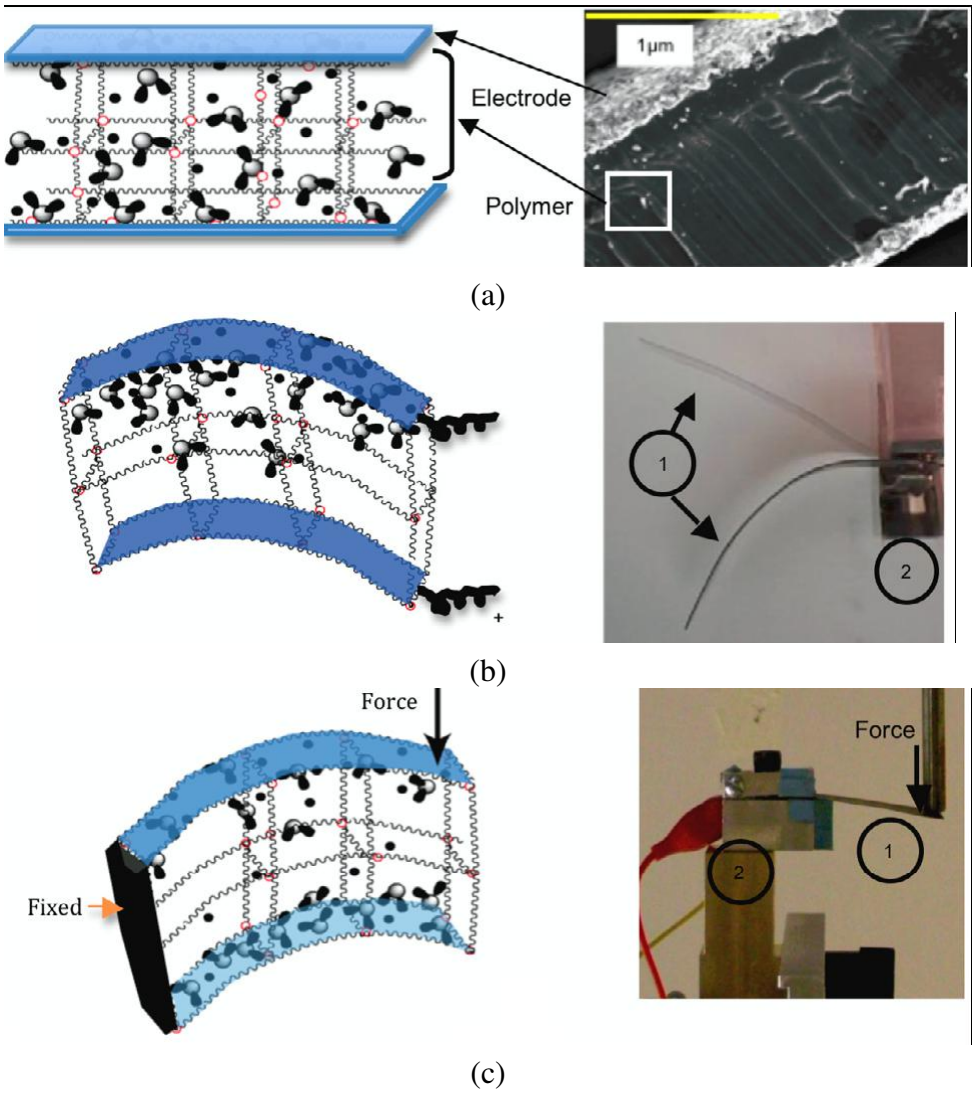

Figure 1.4: Illsutration to show the ions, water and polymer chain inside an IPMC, along with an SEM image of the cross-section when no external input is exerted (a); the electromechanical effect in an IPMC causing the IPMC to bend, with a photograph showing the IPMC bending under electric field (b); and the mechanoelectrical effect due to charge motion on mechanical bending (c) [24].

1.2.1 Properties of IPMCs that make it ideal for use in Flapping Wing Micro Aerial Vehicles

- IPMCs are flexible and exhibit large bending deformation when actuated with electric potential.
- Low weight.
- Low power consumption.
- Wide range of frequencies at which they can be operated.
- Good response.

Chapter 2

Literature Survey

2.1 Flapping Wing MAVs

Unoccupied Air Vehicles (UAVs) have become pervasive in modern warfare by providing real-time intelligence, surveillance and reconnaissance (ISR) to the war-fighter without the limitations and massive logistics footprint of manned flight. Recently, Micro Air Vehicles (MAVs) have been proposed to provide a similar capability in a smaller package. MAVs are autonomous vehicles with a maximum dimension of 15cm or less, weighing 90g or less. They can be easily carried by small combat units and flown in confined spaces such as urban canyons, caves and indoors. MAVs will provide an organic ISR capability to small combat teams in the field, reducing or eliminating their reliance on larger UAVs that are in high demand, and increasing the team's autonomy. MAVs of many shapes and sizes have been proposed but most have either fixed wings, rotary wings or flapping wings. Flapping wing MAVs (FWMAVs) have several advantages over fixed and rotary wing vehicles. They capitalize on several unsteady aerodynamic effects that generate additional lift at the low Reynolds numbers (Re) experienced by vehicles of this size, they have superior maneuverability including the ability to hover, and they mimic biological flyers so they are less conspicuous to potential adversaries.[2]

Autonomous flight vehicles are nothing new. The first UAVs were developed as early as World War I in the form of guided munitions, later expanding their roles into radio controlled target drones, reconnaissance aircraft and glide bombs – forerunners of the modern-day cruise missile. The first radio controlled (RC) aircraft flights in Germany in 1936 led the way to further refinement of small UAVs in the postwar era. The interest in small UAVs was held primarily by RC hobbyists as the military had no meaningful payloads small enough to be carried by such small vehicles. Today this situation is reversed. The rise of Micro Electro-Mechanical Systems (MEMS) technology has enabled the development of micro scale sensors, creating a practical use for smaller air vehicles. Unfortunately, it is not pos-

sible to merely scale down an aircraft to the desired dimensions. As was discovered with the development of MEMS technology, the physics of the small are different from that of the large (for example, friction is more important than gravity). For MEMS technology to progress, researchers had to develop a new understanding of these physics, and develop new techniques for overcoming and capitalizing on them. This is the case with small scale, or low Reynold's Number (Re) aerodynamics today. Re is the ratio of inertial forces to viscous forces, and as scale decreases, volume, and thus, mass and inertia decrease significantly. The accompanying decrease in Re is not merely a changed constant to be accounted for in an equation, it marks a significant change in the flow physics; so significant as to render conventional aircraft flight irrelevant. As scale decreases and the aforementioned viscous forces become more significant, the flow becomes more laminar, the boundary layer becomes critical and drag increases by as much as an order of magnitude while lift changes only slightly. This tends to decrease the aerodynamic efficiency (L/D) of airfoils at small Re. Furthermore, as the vehicle size is further limited, the fixed wing aircraft designer is tempted to use low aspect ratio wings to keep the chord length, and thus, Re as high as possible. Unfortunately, low aspect ratio wings come with their own host of problems, including strong wing tip vortices that increase drag, roll instability and highly nonlinear lift curve slopes. Although scaling down conventional fixed-wing aircraft has resulted in successful MAVs as small as 6 inches, the physics strongly suggest that there is a lower bound for such aircraft.[2]

Despite the difficulties of low Re physics, biology clearly demonstrates that small scale flight is possible. Indeed, two approaches to overcoming low Re physics are rotary and flapping wings, which enable a smaller scale vehicle to fly at a higher Re by moving the wings relative to the body. For example, the bumblebee, bombus terrestris, flaps its wings at approximately 150 hz, which corresponds to a wing velocity of approximately 3.83 m/s at the second moment of area point along the wing span (55% of wing span). So even if the insect has no forward velocity, the wing still moves relative to the air at a Re of approximately 1200. When coupled with forward flight, the wing velocity relative to the surrounding air increases further, giving the insect the benefit of higher Re physics than it would otherwise experience. Rotary wing vehicles also enjoy this benefit of relative wing motion, and they may be a viable solution to the MAV problem, however, they do not share the advantages of unsteady aerodynamic mechanisms that flapping wings experience.[2]

Since biology provides substantial proof that small scale flight is possible, with clear understanding of insect flight, it is possible to develop a flapping wing MAV which can be used to provide real time ISR and perform various other functions.

2.1.1 Applications of MAVs

There are several applications of MAVs:

- Reconnaissance Surveillance
- Defence applications
- Weather forecast
- Wildlife study and photography
- Crowd control Border surveillance
- Traffic monitoring
- Tracking criminals and illegal activities
- Biochemical sensing
- Inspection of pipes

2.2 A deeper understanding of IPMCs

2.2.1 Manufacturing and Synthesis

As mentioned before, an IPMC consists of a thin ionomeric membrane sandwiched between metal electrodes that impart a layered structure to the IPMC. The electrodes act as conductive paths for the current flow during sensing. Similarly, the electrode layer intensifies the electric field applied during actuation, thus improving the ion transport inside the polymer membrane. The process of depositing electrodes on the membrane is defined as electroding.

Irrespective of the method used, electroding must -

1. Deposit metal or metal particles close to the membrane surface.
2. Maximize the interfacial area between the membrane and the electrode for maximizing both the electrochemically active surface area and the adhesion.
3. Minimize the electrical resistance of the electrode.
4. Form a uniform metal layer that is chemically and mechanically stable and does not lose adhesion on hydration.

Due to the non-conductive nature of polymers, conventional electroplating techniques cannot be used directly. Hence, various electroding techniques have been researched that satisfy the above criteria. These techniques are broadly classified into chemical and mechanical plating methods. There are distinguishing features between the two techniques. While chemical methods are preferred due to the better adhesion of the electrode to the polymer layer, these methods are time consuming and more expensive. Mechanical techniques are alternatives to chemical techniques and are preferred for deposition of non-precious metals on the polymer membrane. Although mechanical techniques form a uniform electrode, they do not function well in the hydrated state.

2.2.2 Chemical Plating Methods

Chemical plating methods or electroless deposition are used for coating metal electrodes by reducing the metal particles inside the membrane with the aid of reducing agents like sodium borohydride. An early chemical deposition process was reported by Takenaka et al. [28]. This method is commonly known as 'reductant permeation (RP)'. In RP the cationic reducing agent is allowed to diffuse through the membrane on one side, to react with an anionic salt of the metal diffusing from the other side of the membrane. The process has been used for plating platinum, rhodium, iridium, ruthenium and palladium. Another method, 'impregnation–reduction (IR)', similar to RP, was later reported by Millet et al. [16, 15] for plating platinum onto a Nafion® membrane. In the IR process, the cation of the metal is incorporated inside themembrane and later reduced using a reducing agent. IR has been observed to be superior to RP as it can form durable metal electrodes easily.

The manufacturing process of electroless deposition (IR) is as follows -

1. The Nafion® membrane is hydrated in DI (de-ionized) water for 24 h and cleaned in a water bath.
2. The cleaned sample is then immersed in a platinum salt solution for 2 h.
3. The reduction process using ammonia and sodium borohydride follows; these are added every half hour, with the bath temperature increasing from 40 to 70^{o}C (reduction temperature).
4. The reduction process is repeated until a surface resistivity less than 10 /sq is achieved.

This deposition method typically results in IPMCs with thickness between 0.17 and 0.20 mm and an approximate electrode thickness of a few micrometers (1–5 μm) each.

Kim and Kim [12] have also observed an improvement in IPMC actuation by sequentially reducing palladium and platinum on Nafion® by the IR method. A displacement of 7.8 mm by 2 V DC actuation with no back relaxation was observed for a sample with dimensions of 10mm×50mm×0.2mm. Also an improvement in blocking force was observed (0.125 g for a Pd–Pt IPMC, 2 V DC). These improvements could be explained by the electrode morphology. The palladium IPMC was observed to have lower electrode resistivity. In addition, the surface morphology of the Pd–Pt electrode was observed to be more uniform than the platinum coated IPMC. This in turn is expected to reduce current consumption thereby producing uniform electric field.

Electroless deposition by RP and IR is the most commonly used manufacturing process as it produces mechanically and chemically stable electrodes. Variation of the reducing agent concentration can control the electrode thickness. However, some modifications of RP and IR have been reported in recent years and are as follow -

1. Reverse electroless plating has been reported by Chung et al. [5] for plating platinum on Nafion®. The membrane is first immersed in 5 wt% NaBH4 for 12 h followed by subsequent immersion in (Pt(NH3)4)Cl2. The reverse electroless plating results in a smaller average particle size and more uniform distribution of metal particles in the membrane. A surface roughness of 3 nm was observed for reverse electroless plating as compared to 52 nm for the IR process. In addition, the platinum penetration inside the membrane through reverse plating was observed to be more than that of the typical process.

2. Bennett and Leo [3] reported the fabrication of IPMCs with non-precious metals in combination with noble metals by co-reduction. A lifecycle of 250 000 cycles was achieved by co-reduction of copper and platinum (Cu–Pt) inside a Nafion® membrane. The metal particle distribution and interfacial area could be controlled by varying the proportions of precious and non-precious metal ion concentrations inside the membrane before reduction. It was observed that the stability of the Cu–Pt electrode was dependent on the platinum proportion in the electrode. The resistance of the electrode was measured to be between 6 and 11 cm−1.

Although chemical plating methods produce mechanically stable electrodes, they are time consuming, complex, expensive and need adjustment for different metals and membranes. Hence, mechanical plating techniques are sometimes used.

2.2.3 Mechanical Plating Methods

Mechanical plating methods have been adopted as simple and quick alternatives to chemical plating methods.

Three main techniques are widely used for electroding -

1. **Physical Vapour Deposition (PVD)** especially sputter coating, is the most commonly used mechanical deposition technique. Sputter coating has either been used independently or in conjunction with other techniques like electroplating, electroless deposition and plasma etching. Sputter coating provides an easy means of electrode deposition, at the same time reducing the manufacturing time to a few hours as compared with 24 h in the chemical deposition technique. Different metals like gold, platinum, titanium, nickel and silver can be deposited without extensive alteration of the technique. Also the thickness and roughness of the coated electrode can be easily controlled. Sputter coating on IPMCs manufactured by the IR process was observed to improve the tip displacement and force [14]. However, since the sputtering is performed on dry samples, delamination on hydration is frequently observed. Also, sputter-coated samples are prone to cracking on usage.

2. **Solution Casting** is used for either electroding or increasing the polymer thickness. For electroding purposes, a Nafion® solution is mixed with conducting powders like carbon, silver, palladium, platinum, copper or gold [11]. The electrode is cured under elevated temperature for stability. Solution casting of Nafion® has been employed to attain thicker polymer layers. A thickness of 0.4–1.2 mm has been achieved [9]. While increased thickness enhances the blocking force, the displacement, on the other hand, is reduced. Typically, an IPMC is used in the bender configuration. Solution casting, however, provides a means to fabricate different shapes of the transducer.

3. **Hot Pressing:** In order to achieve a particular thickness of themembrane, the process of solution casting needs to repeated a few times; hence an alternate method of hot pressing Nafion® membranes has been used. Hot pressed Nafion® pellets have also been commonly used for fabricating different shaped transducers [30, 1]. However, the pellets need to be activated chemically and have been observed to lose flexibility along the way.

4. **Direct Assembly Process** has been developed for electroding dry and solvated membranes [22]. Electroding is performed by directly painting the electrode solution either on the membrane or on Furon before hot pressing it onto the membrane at 210^oC and 20 MPa pressure to improve the adhesion between the electrode layers and the

membrane. Initial painting on Furon provides better control of the conductor loading and electrode uniformity. Highly conductive electrodes (1–20 S cm−1) have been achieved using the DAP. Direct painting has been observed to lead to wrinkles in the membrane due to solvent absorption. No intermediate layer is observed. Also, adhesion of the conductive surface on the high surface area electrode was observed to cause performance degradation.

It should be noted that the choice of a particular technique for IPMC fabrication is based on the quality and stability of the electrode, cost and time of fabrication and the specific application.

2.2.4 Microstrucure

IPMCs made from Nafion 117 (i.e., 1,100 g per mole sulfonate dry membrane of 178 μm thickness, the metal-plated composites being close 200 μm in thickness) consist of the following constituents: [17]

1. backbone perfluorinated copolymer of polytetrafluoroethylene with perfluorinated vinyl ether sulfonate pendants, forming interconnected nanoscale clusters that contain the sulfonates and their neutralizing cations;
2. electrodes consisting of 3–10 nm in diameter metal (generally platinum) particles, distributed mainly within 10–20 mm depth of both faces of the membrane, and usually covered with 1–5 mm gold plating;
3. neutralizing cations; and
4. a solvent, usually water.

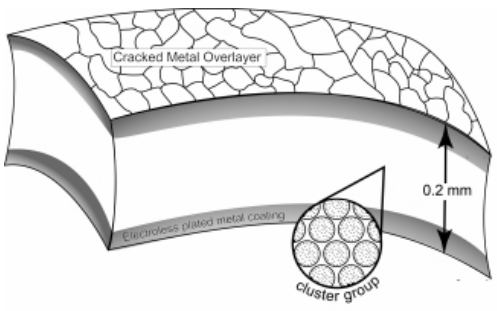

Figure 2.1: IPMC schematics indicating surface morphology, interface, and cluster structure.

The backbone Perfluorinated ionomers that are generally used in IPMC manufacture include Nafion, Flemion, and Aciplex. Based on the ionomers used IPMCs exhibit unique deformation behavior when subjected to electric voltage across their electrodes. For example, when subjected to a step voltage, the initial fast displacement is generally followed by a slower relaxation, in the reverse direction for Nafion-based IPMCs and in the same direction for Flemion-based IPMCs.[19] Further, when the two faces of the strip are shorted during this slow relaxation, a sudden fast motion, in the same direction for Nafion-based and in the opposite direction for Flemion-based IPMCs, was found to occur. [19] Also these ionomers appear as clusters in the polymer membrane, the sizes and nature of which, determine the magnitude of deformation for a given voltage in a IPMC. [17]

The surface electrodes are responsible for electrical contact and play a major role in the performance of IPMCs. Noble metals such as Pt, Au and Ag are preferred as elctrode materials due to requirements such as low chemical reactivity and high electrical conductivity. The metal surface in an IPMC usually appears fractured, displaying discrete islands of metal deposition between 5–20 μm across. It is presumed that water swelling and electroactive bending generate these islands when the resulting strains exceed the tensile strength of the thin metal layer. [19]Surface resistance [27] and nature of the surface electrode [22] also play a critical role in the performance of IPMCs.

Various neutralizing cations that can be used are - H^+, Li^+, Na^+, K^+, Rb^+, Cs^+, Ti^+, Ba^+, and several organic cations such as TBA^+ (tetrabutyl ammonium) and TMA^+(tetramethylyl ammonium). Remarkably, the stiffness of the bare polymer as well as that of the corresponding IPMC changes with the cation type for the same membrane and at the same level of solvent uptake (e.g., hydration), as well as with the degree of solvent uptake. The amount of solvent uptake at full saturation depends on the cation used, being a maximum for H^+. It also depends on the temperature and duration of the solvent-uptake process.[17]

2.2.5 Actuation Mechanism

Actuation in IPMC samples is believed to be achieved due to the migration of hydrated ions in the polymer membrane when an electric potential is applied across it's electrodes. When a low voltage electrical field (1 – 5V) is applied, the transport of hydrated cations within the solvated IPMC and the associated electrostatic interactions lead to bending motions of the IPMC sheet. Thus, an IPMC can work as a small size actuator. Figure 3 illustrates the mechanism of the IPMC as actuator. On the other hand, when an IPMC is mechanically bent, it will generate a low voltage (order of milivolts) between the two electrodes. The generated voltage is due to the non-uniform concentration of ions in the IPMC membrane. Figure 4 illustrates the behavior of the IPMC as sensor. [13] The bending deformation observed is

believed to be a result of volumetric strain induced in the material when the bulk of hydrated ions migrate towards the cathode during the application of a suitable electric potential across the elctrodes.

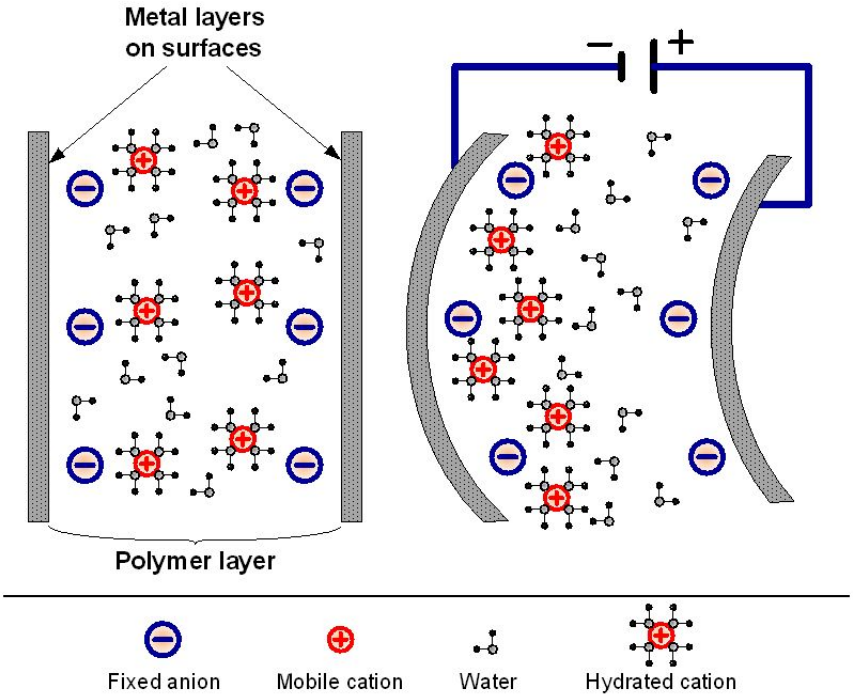

Figure 2.2: Operating principle of IPMC as actuator [13]

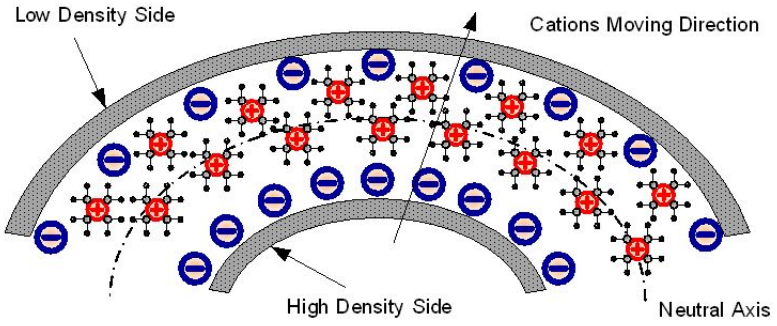

Figure 2.3: Fundamental of IPMC as a motion sensor [13]

According to another model Ion migration in the polymer membrane is believed to generate osmotic imbalance within the layer. When this osmotic pressure is high enough to overcome the elastic stiffness of the IPMC sample bending is believed to occur. [19]

2.2.6 Properties and Characterization of IPMCs

2.2.6.1 Polymer Properties

As seen earlier, the functional properties of the polymer membrane used dictates the functionality and performance of the IPMC. Besides the polymer units present in them tend to

exist in the form of clusters with constant spacing (generally of the order 5nm for Nafiaon IPMC samples [25, 32]) the magnitude of which is dependent on water content. Upon hydration, it has been noted that the total number of clusters decreases while the size of each cluster increases, suggesting a cluster-consolidation model for Nafion hydration [4, 19]. The cluster size directly affects dipole interaction and molecular interaction, thereby significantly influencing the electrical properties as well as mechanical stiffness of the IPMC.

2.2.6.2 Ion-Exchange Capacity

The ion-exchange capacity of an IPMC material indicates the number of sulfonate (Nafion) or carboxylate (Flemion) groups within a fixed volume of material. [19] This number should correspond to the number of substituted (non-H^+) charge-balancing cations within the IPMC. Since the migration ions, under the influence of an applied voltage, is responsible for bending or actuation in an IPMC, the equivalent weight of the ions in the composite is of importance. The equivalent weight of ions in an IPMC is given by -

$$EW_{ion} = \frac{EW_{H^+} - 1.008 + FW_{ion}}{SF}$$

where EW_{H^+} is the equivalent weight of the dry ionomer in proton form (1100 for Nafion117), 1.008 is the formula weight of the proton in grams per mole, FW_{ion} is the formula weight of the cation used, and SF is a scaling factor which accounts for any added electrode mass (typically around 0.5 - 0.65)[19, 17]

2.2.6.3 Solvent Content and Swelling

The solvent content influences many functional aspects of an IPMC sample, which include properties such as ion exchange rate, ionomer cluster size and mechanical stiffness. If water is used as the solvent, it also boosts the H^+ content in the polymer membrane. This can be avoided with the use of organic solvents, but, they can limit the free movement of ions. The maximum solvent pressure in an IPMC sample before failure is also a measure of the elsatic stiffness of the sample. [19, 17]

2.2.6.4 Ion Migration Rates

It has been shown that the diffusion of alkali metal ions through Nafion membranes varies with the ion used. At high concentration, it has been shown that the rate of diffusion is in the order $Li^+ < Cs^+ < Rb^+ < Na^+ < K^+$ for alkali metals, $Ca^{2+} < Ba^{2+} < Sr^{2+}$ for alkali earth metals, and $Y^+ < Ca^{2+} < Na^+$ for ions of similar ionic size (0.93-0.99 Å) but different charge. At low metal concentrations, the transport rate is controlled by boundary layer diffusion and the metal flux follows the order $Li^+ < Na^+ < K^+ < Rb^+ < Cs^+$ for alkali metals, and $Ca^{2+} < Sr^{2+} < Ba^{2+}$ for alkaline earth metals [31]. Ion motion occurs in tandem with water migration, either through primary solvation, shell migration of water or

other solvent molecules, or through secondary electro-osmotic migration of water. [19]

2.2.6.5 Metal Content and Distribution

The distribution and morphology of deposited metal at the surface of IPMC materials has a significant effect on their actuation behavior. Performance of IPMCs as actuators correlates with their surface morphology, with the best electrodes for IPMC actuators being those that exhibit the largest available surface area and greatest surface conductivity[19]. It has also been demonstrated that the formation and growth of the nanothorn assemblies at the electrode interface lead to a dramatic improvement (3- to 5-fold increase) in both actuation range and blocking force at low driving voltage (1–3 V). [21]

2.2.6.6 Stiffness

Nafion polymers are viscoelastic, exhibiting first-order tensile moduli from 50–1500 MPa and greater. The variation in stiffness is attributed to the action of ions within the membrane increasing stiffness by acting as cross-linking agents [6]. The stiffness of dry IPMC samples correlates with the radius of the alkali metal countercation (Li+, Na+, K+, Rb+, Cs+, and Tl+). Smaller cations may more closely approach the sulfonate anion, yielding a smaller ion pair dipole (6). Larger dipoles in interaction will require a greater energy for reorganization. This can result in a larger observed stiffness of the material [7, 19]. Several mathematical and experimental methods have been developed over the year to compute the stiffness of IPMC systems, but experimental models are the most reliable at the moment due to a lack of complete understanding in the nature and mechanical behaviour of IPMCs.

2.2.7 Advantages / Disadvantages of IPMCs

Several propertries and charecteristics of IPMCs that either serve as advantages or disadvantages for typical applications are discussed below. [19]

- The tip force or power generated during actuation for IPMCs (about 10 Wkg^{-1}) is relatively less compared to muscle fibres (about 1000 Wkg^{-1}) , pneumatic, hydraulic or piezoelectric components.
- IPMCs require very little power for actuation and voltages as low as 1V can be used to obtain actuation. The magnitude of deformation obtained increases with increase in applied voltage but application of voltages above a certain threshold can lead to electrolysis of water and hence losss in solvent content and hydration. This threshold voltage is about 1.23 V for IPMCs with Platinum electrodes and is relatively higher for IPMCs with non-platinum electrodes, as they are more easily polarized and develop an overpotential that increases the voltage required for water electrolysis.

- IPMCs need to be hydrated in order to function effectively as hydrated cations are the precursors for actuation or sensing in them. This also limits the maximum voltage that could be used as input in order to avoid electrolysis of water/solvent. Nafion ionomers are compatible with a large number of organic solvents having higher electrolytic voltages. Unfortunately, it is expected that the lower conductivity of these organic solvents will have a detrimental effect on IPMCs' overall force generation.
- Due to the equilibrium nature of ion exchange in ionomeric polymers, care must be taken to prevent sample contamination when IPMCs are operated in the presence of any competing cationic species (such as salt water). For example, a sample prepared in the lithium form will rapidly exchange with sodium ions if available. Since power output in sodium IPMCs is less than in lithium samples, sample composition is an important parameter that must be considered
- IPMCs are expensive to manufacture. The electrode material, which should ideally be a noble metal such as Platinum, Gold or Silver, is in itself quite expensive. The electro-active polymers used in IPMCs, such as Nafion or Flemion, are also expensive.
- IPMC materials suffer from their lack of rigidity. Further processing of IPMCs is delicate and may lead to variations among samples produced. These variations including surface morphology, small bends, ripples, and other processing imperfections can yield large variations in actuator performance.
- IPMCs exhibit bending mode of actuation and hence donot accurately represent the term "artificial muscles". They are not suitable for use in applications involving linear actuation.
- Natural muscles consist of millions of strands of individual muscle fibers. IPMC materials studied to date are large (1–10-mm wide) and are operated as single slabs. A combination of multiple pieces to form IPMC bundles could be used to scale the performance of these materials. This engineering challenge requires electrical connections between IPMC slabs that prevent short-circuiting between slabs and lubricate the contact between neighboring slabs.

2.2.8 Application of IPMCs in Flapping Wing MAVs and other Bio-mimetic Robots

2.2.8.1 Bio-mimetic Robotic Fish [4]

Chen et al. have have proposed a physics-based model of a bio-mimetic robotic fish propelled by an ionic polymer–metal composite (IPMC) actuator. Inspired by the biological fin

structure, a passive plastic fin was further attached to the IPMC beam. The model incorporated both IPMC actuation dynamics and the hydrodynamics, and predicted the steady-state cruising speed of the robot under a given periodic actuation voltage. The interactions between the plastic fin and the IPMC actuator were also captured in the model.

2.2.8.2 A Bio-mimetic Jellyfish Robot [33]

A bio-mimetic jellyfish robot based on ionic polymer metal composite actuators was fabricated and activated to mimic real locomotive behavior with pulse and recovery processes by . To imitate the curved shape of the jellyfish, a thermal treatment was applied to obtain a permanent initial deformation of a hemispherical form. The bio-inspired input signal was generated for mimicking real locomotion of the jellyfish. The vertical floating displacement and the thrust force of the bio-mimetic jellyfish robot under various input signals were measured and compared. The present results show that the bio-inspired electrical input signal with pulse-recovery process generates much higher floating velocity of the bio-mimetic jellyfish robot in comparison with pure sinusoidal excitations. The curved shape of the IPMC actuator through thermal treatments can be successfully applied to mimic the real bio-mimetic robots with smooth curves.

2.2.8.3 Tadpole robot [21]

Researchers Kim Byungkyu, Kim Deok-Ho, Jung Jaehoon and Park Jong-Oh Park have developed a wireless undulatory tadpole robot using ionic polymer–metal composite (IPMC) actuators. In order to improve the thrust of the tadpole robot, a bio-mimetic undulatory motion of the fin tail was implemented. The overall size of the underwater microrobot prototype, shaped as a tadpole, wass 96 mm in length, 24 mm in width, and 25 mm in thickness. It had one polymer fin tail driven by the cast IPMC actuator, an internal (wireless) power source, and an embedded controller. The motion of the tadpole microrobot was controlled by changing the frequency and duty ratio of the input voltage. The frequency range used was 1Hz - 8Hz. Experimental results have shown that this technique can accurately control the steering and swimming speed of the proposed underwater tadpole robot. The rabot was able to achieve a maximum speed of $23.6 mms^{-1}$ at a 4 Hz driving frequency.

2.2.8.4 Flapping Wing MAV using IPMC [10]

Researchers at the Department of Aerospace Engineering, Korea Advanced Institute of Science and Technology, Daejeon, Republic of Korea designed and manufactured a working model of a flapping wing MAV wing actuated with IPMC strips manufactured from Nafion with Pt electrodes. The wings, manufactured from PET films, were attached to the tips of an IPMC actuator directly as shown in Fig. 1, and the flapping actuator module was actuated at the 1st natural frequency to increase the actuating frequency and the flapping angle.

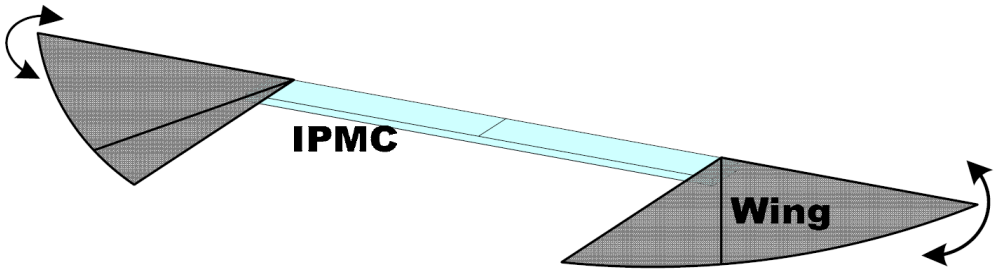

Figure 2.4: Schematic diagram of the flapping actuator module developed using IPMC.[10]

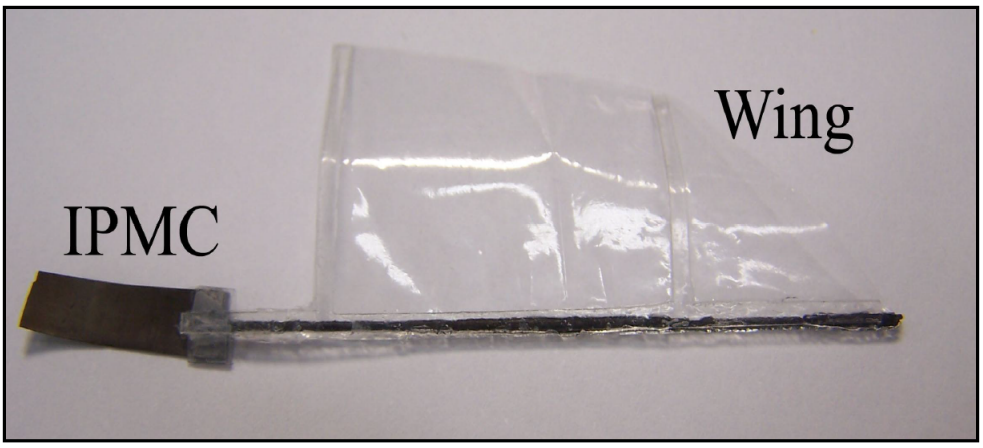

Figure 2.5: Picture of the flapping actuator module[10]

The wing weighed about 0.040g with a length of 40 mm and a surface area of $7cm^2$. The IPMC strip used on the other hand measured $20mm \times 5mm \times 0.205mm$. These dimensions were chosen to mach that of a butterfly. Through experimentation the natural frequency of the developed wing was found to be 4.75 Hz. For the final testing Kim *et al*. used a 2.5V and 4.75Hz sinusoidal signal as input. The model was found exhibit successful flapping motion with a flapping angle of about 36 but suffered from a few discrepancies.

The wing was only able to generate a mean lift of 0.00258gf, the maximum and minimum lift being 0.0361gf and -0.0313gf respectively, which was much smaller than the total mass although only one wing was used to measure the lift. Kim et al. attributed this lack in lift to the low 1st natural frequency and the relatively small flapping angle. The typical butterfly used as an inspiration for the work could flap at a much higher frequency of about 10.5 Hz and achieved much higher flapping angles. Generally, the phase angle between the flapping angle and the lift is approximately 90° as the maximum lift is generated when the flapping angle is 0° during the down stroke. Further the phase angle between the flapping angle and the lift for the test was found to be nearly 39.6°, which is much lower than the typical 90° , observed in nature, as the maximum lift is generated when the flapping angle is 0° during the down stroke. This discrepancy in flapping angle was a result of the large contribution of inertia forces in the measured lift, which was later confirmed by repeating the experiments

with only the wing frame intact. A butterfly wing typically weighs about 10% of it's entire mass which is typically around 0.128g, whereas the IPMC wing used for testing weighed much higher at 0.04g.

These discrepancies can be overcome by choosing lighter materials for the wing frame coupled with a better design to increase the 1st natural frequency to desirable levels. Further design considerations should be made to achieve higher flapping angles and higher frictional component in the measured lift.

Chapter 3

Aim and Scope of Present Work

3.1 Aim of Present Work

Researchers have developed flapping wing mechanisms which mimic the wing movements of birds. Light flapping micro aerial vehicle using electrical-discharge wire-cutting technique. Several flapping wing mechanisms which mimic an insect's wingbeat kinematics have been developed. These mechanisms have greatly helped in increasing the fundamental understanding of flapping flight. Unfortunately, these dynamically scaled flapping wing mechanisms are bulky and flap at very low frequency. Therefore, they may not be suitable for use in small or micro-scale flying vehicles. Moreover, current flapping wing mechanisms rely on pneumatic and motor-driven flapping actuators which lead to high weight and system complexity. Additionally, it may not be easy to mimic the complex wingbeat kinematics of the natural flyers with these conventional actuators. Another plausible alternative for developing flapping wings is to use actuators made of smart materials.Ionic Polymer metal composite is a type of smart material which has developed recently.

The aim of the present work is to establish and show that IPMC material can be used as an actuator for a flapping wing MAV by designing and analyzing the wing, and also suggest optimal dimensions of the IPMC actuator strip.

3.2 Approach of Present Work

The approach of the present work is three fold

- Complete literature survey to understand flapping wing MAVs using smart material as actuators, problems faced in developing them, various actuation mechanisms previously used, design of the MAVs from biomimetic inspirtaion.From literature of previous work, we have taken inspiration from **Dragon Fly**. The Dragonfly **wingspan varies from 2.63 cm to 19.0 cm** across it's different species. Natural frequencies of some of the species of dragonfly are listed in the table.

	Total mass (mg)	Beating frequency (Hz)	Natural frequency (Hz)
Anax parthenope julius	670	27	75/120
Cercion calamorum calamorum	27	41	133
Sympetrum baccha matutinum	191	31	67
Calopteryx atrata	245	15	48

- Second is to choose suitable materials for the wing and modelling it. As per the literature survey done, **Poly Ehtyl Ether Ketone (PEEK)** for the frame of the wing and **Mylar film** were chosen. PEEK is preferred over Carbon Rods because it has higher density and is isotropic in nature, thus simplifying the analysis process. The wing is modelled in commercial modelling software, Autodesk Inventor.
- Finally, a multiphysics software, Comsol Multiphysics® is used to predict the deformation of the wing attached to the IPMC strip and various other parameters such as surface stress, frequency of flapping etc.

3.3 Scope of Work

It comprises of the following

1. Full literature survey about flapping wing MAVs and IPMCs.
2. Biomimetic inspiration and selection of suitable materials for design and analysis.
3. Modelling the wing frame.
4. Using the multiphysics software to couple the IPMC strip to the wing.
5. Computer simulation for prediction of deflection of the wing and other properties.
6. Drawing conclusions and making recommendations.

Chapter 4

Research Methodology

4.1 Design

Having taken inspiration from dragonfly and the design of the wing is done.. The design phase is started by choosing the physical structure of the wing. The wing we narrowed down to has a frame made of **Poly Ethyl Ether Ketone (PPEK)** and attached to **Mylar film**, alongwith this, it consists an **IPMC strip** attached to its root. The IPMC strip is attached to the root of the wing on one end and clamped to the body of the MAV (not shown in figure) on the other end. The basic structure of the wing is shown in Figure-2. The frame along Z-axis is 0.5 mm thick. The wingspan is 7.1 cm, thickness of the main rib is 1.0 mm and the thickness of the ribs running along the membrane is 0.75 mm. The width and thickness of the root of the wing are 3.5 mm and 0.5 mm respectively. The thickness of the mylar fillm generally varies between 10-30 microns. For our model, we have taken a mylar film of thickness 30 microns but it won't be visible in the model since it is in 2-D.

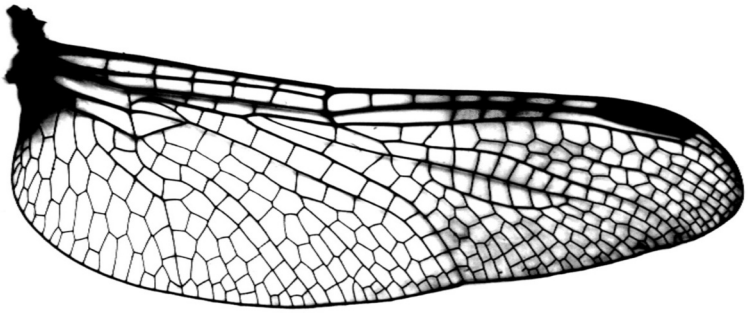

Figure 4.1: Dragonfly Wing

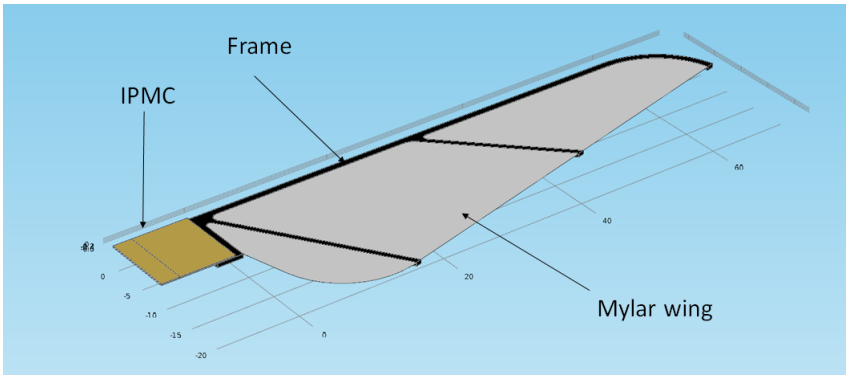

Figure 4.2: Basic Wing Structure

4.2 Electrochemical Analysis

We developed a 3D actuation model for the IPMC. The model will be developed in a software package known as Comsol Multiphysics®. A discussion is made in regards to the force coupling methodology necessary for the future steps of the study.

4.2.1 Ionic Model

The following section defines the equations explicitly used in order to numerically solve the physical phenomenon. Cation transport within the polymer is calculated with the Nernst-Plank equation

$$\frac{\partial c}{\partial t} - \nabla.(D\nabla c + z\mu F c\nabla V) = 0 \tag{4.1}$$

where cεR is the cation concentration, D is the diffusion coefficient, F is the Faraday constant, z is the charge number, $\mu$is the cation mobility, V ε R and is the electric potential in the polymer. Applied voltage causes all free cations to migrate towards the cathode. Since the anions are fixed to the polymer backbone, the equation solves for strictly cation concentration. Because cations cannot leave the polymer domain, concentration begins to converge near the electrode polymer interface. This in turn increases the electric field.

$$-\nabla^2 V = \frac{\rho}{\varepsilon_o \varepsilon_r} \tag{4.2}$$

where V is considered to be the potential in the polymer, and $\varepsilon_o\varepsilon_r$is the dielectric permittivity. The space charge density is defined in order to affect the electric field as follows

$$\rho = F(c - c_c) \tag{4.3}$$

where $c_o$is assumed the constant anion concentration. In this study, the electric field propagation down the electrode length is simplified. Rather than using Ohm's law to determine the electric current propagation, the electrode domain was partitioned near the location of the voltage source. This implementation was used in order to simplify the electrodynamics in order to investigate the solid mechanics more effectively. The electrode surface is still taken into consideration because the platinum domain stiffness cannot be neglected when analyzing the solid mechanics.

4.2.2 Mechanics Model

In order to link the deflection with the cation transport force coupling was done. A basic linear elastic model was used in order to quantify the mechanical behavior of the IPMC. The following equation describes the strain relationship with respect to the deformation

$$\varepsilon = \frac{1}{2}(\nabla u^T + \nabla u) \tag{4.4}$$

where $\varepsilon\ \varepsilon\ R^{6x6}$ is the strain tensor, and u $\varepsilon\ R^3$is the displacement vector.

If the differential operator D is expressed in matrix form rather than a gradient operator ∇, the Cauchy strain tensor can be expressed in matrix form as follows

$$\begin{bmatrix} \varepsilon_{11} \\ \varepsilon_{22} \\ \varepsilon_{33} \\ \varepsilon_{12} \\ \varepsilon_{23} \\ \varepsilon_{13} \end{bmatrix} = \begin{bmatrix} \frac{\partial}{\partial x} & 0 & 0 \\ 0 & \frac{\partial}{\partial y} & 0 \\ 0 & 0 & \frac{\partial}{\partial z} \\ \frac{\partial}{\partial y} & \frac{\partial}{\partial x} & 0 \\ \frac{\partial}{\partial z} & 0 & \frac{\partial}{\partial x} \\ 0 & \frac{\partial}{\partial z} & \frac{\partial}{\partial y} \end{bmatrix} \begin{bmatrix} u \\ v \\ w \end{bmatrix} \tag{4.5}$$

which can be expressed as

$$\varepsilon = Du \tag{4.6}$$

The stress strain relationship is noted by the following equation

$$\sigma = E\varepsilon \tag{4.7}$$

where $\sigma\varepsilon R^{6x6}$ represents the general stress tensor for three dimensional space, $E\varepsilon R^{6x6}$ is the elastic stiffness matrix. This simulation implements a standard linear elastic model for the solid mechanics, thus the stiffness matrix is explicitly of the following form

$$E = \frac{E}{(1+\nu)(1-2\nu)} \begin{bmatrix} 1-\nu & \nu & \nu & 0 & 0 & 0 \\ \nu & 1-\nu & \nu & 0 & 0 & 0 \\ \nu & \nu & 1-\nu & 0 & 0 & 0 \\ 0 & 0 & 0 & 1-2\nu & 0 & 0 \\ 0 & 0 & 0 & 0 & 1-2\nu & 0 \\ 0 & 0 & 0 & 0 & 0 & 1-2\nu \end{bmatrix} \begin{bmatrix} \varepsilon_{11} \\ \varepsilon_{22} \\ \varepsilon_{33} \\ \varepsilon_{12} \\ \varepsilon_{23} \\ \varepsilon_{13} \end{bmatrix} \tag{4.8}$$

where is the E elastic Young's modulus, and ν is the Poisson's Ratio. Substituting this in equation 7, the volumetric force equation can be described at equilibrium as follows

$$-D^T \sigma = F_V \tag{4.9}$$

Where $F_V \varepsilon R^3$represents the body force per unit volume.

In a paper which was written by D. Pugal et al., they proposed that the calculation of the body force should be implemented more precisely in 3D by the following equations (where α and β are empirically found constants)

$$F_{V;cathode} = \alpha \rho_s^2 \tag{4.10}$$

$$F_{V;anode} = \beta \rho_s \tag{4.11}$$

where the quadratic term applies only to the neighborhood about the cathode and the linear term applies to the neighborhood about the anode.

The above equations can be simplified and written in a general form as[23]

$$\alpha_2 \frac{sgn(\rho)+1}{2} \rho_s^2 \; - \; \beta_2 \frac{sgn(\rho)-1}{2} \rho_s \tag{4.12}$$

The issue with the implementation of this force coupling model is that it requires previous knowledge about where the potential is being applied. This is not necessarily the case for the design optimization. In some cases, the applied voltage location is used as a variable in order to produce an optimal design output. In order to correct the direction for three-dimensional implementation as well as maintain robust consistency when running design optimization, the original equation was augmented as follows

$$F_V = \frac{\nabla c(\alpha \rho_s + \beta \rho_s^2)}{||\nabla c||} \tag{4.13}$$

where ∇c is concentration gradient. In vector form it becomes the following

$$F_V = \frac{(\alpha\rho_s + \beta\rho_s^2)}{\sqrt{(\frac{\partial c}{\partial x})^2 + (\frac{\partial c}{\partial y})^2 + (\frac{\partial c}{\partial z})^2}} \begin{bmatrix} \frac{\partial c}{\partial x} \\ \frac{\partial c}{\partial y} \\ \frac{\partial c}{\partial z} \end{bmatrix} \tag{4.14}$$

This method was used to direct the body force appropriately. This is done by normalizing the magnitude of the concentration gradient while maintaining the direction.

4.3 Modelling in COMSOL

A $10mm \times 10mm \times 0.2mm$ IPMC strip was modeled and was analyzed along with the imported structural wing design on Comsol Multiphysics®.

4.3.1 Pre-Processor

The simulation parameters to were first setup as follows.

Si. No.	Name	Value [units]	Description
1	F	96458 $[Cmol^{-1}]$	Faraday Constant
2	ε	0.02 $[Fm^{-1}]$	Dielectric permittivity (polymer)
3	C_0	1200 $[molm^{-3}]$	Initial Cation Concentration
4	D	7×10^{11} $[m^2s^{-1}]$	Diffusion Coefficient
5	α_2	70 $[Nm^4mol^{-2}]$	Quadratic Force Coupling
6	β	1×10^5 $[Nmmol^{-1}]$	Linear Force Coupling
7	z	1.0	Cation Charge Number
8	T	293 $[K]$	Temperature

Next a set of variables, as shown in the table below, were defined for use in the simulation.

Si. No.	Name	Expression	Description
1	V_{pos}	$1.0(\sin(2\pi t))$ $[V]$	Voltage Source
2	V_{neg}	0 $[V]$	Ground
3	r	$\frac{1\times0.02}{1.1125}$ $[\Omega m]$	Resistivity (Pt electrode)
4	ρ	$F(C-C_0)$ $[Cm^{-3}]$	Charge Density
5	ρ_s	$C-C_0$ $[molm^{-3}]$	Change in Cation Concentration
6	F_Z	$\alpha_2\frac{sgn(\rho)+1}{2}\rho_s^2 - \beta_2\frac{sgn(\rho)-1}{2}\rho_s$ $[Nm^{-2}]$	Body Force in the Z-direction

The material properties for use in the simulation were also input as follows.

Si. No.	Name	Young's Modulus, E $[Nmm^{-2}]$	Poisson's Ratio, ν	Density, ρ_m $[kg/m^3]$
1	Nafion (polymer)	41	0.49	2600
2	Epoxy Adhesive (electrode)	723	0.44	1280
3	Mylar	3790	0.35	1400
4	PEEK	3600	0.38	1320

4.3.1.1 Geometries

Two Geometries were set up for the simulation. The first Geometry was set up in order to solve the electro-chemical ion transport problem. This included a $10mm \times 10mm \times 0.2mm$ Nafion Polymer film sandwiched between two layers of Platinum electrodes of $8\mu m$ thickness, modeled in 2D.

In the earlier a 3D model was attempted for the IPMC strip but was later replaced by a more effecient 2D model. This was possible as no significant change in the value of variables were observed along one width of the strip (the y-axis in the 3Dmodel). This is illustrated in the figures below.

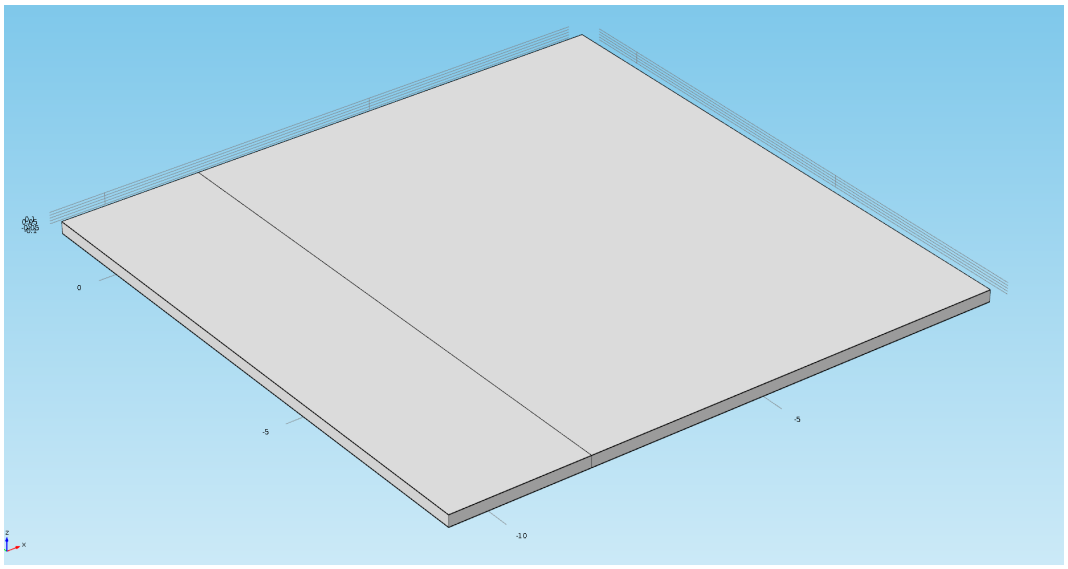

Figure 4.3: IPMC Strip initially modelled in 3D

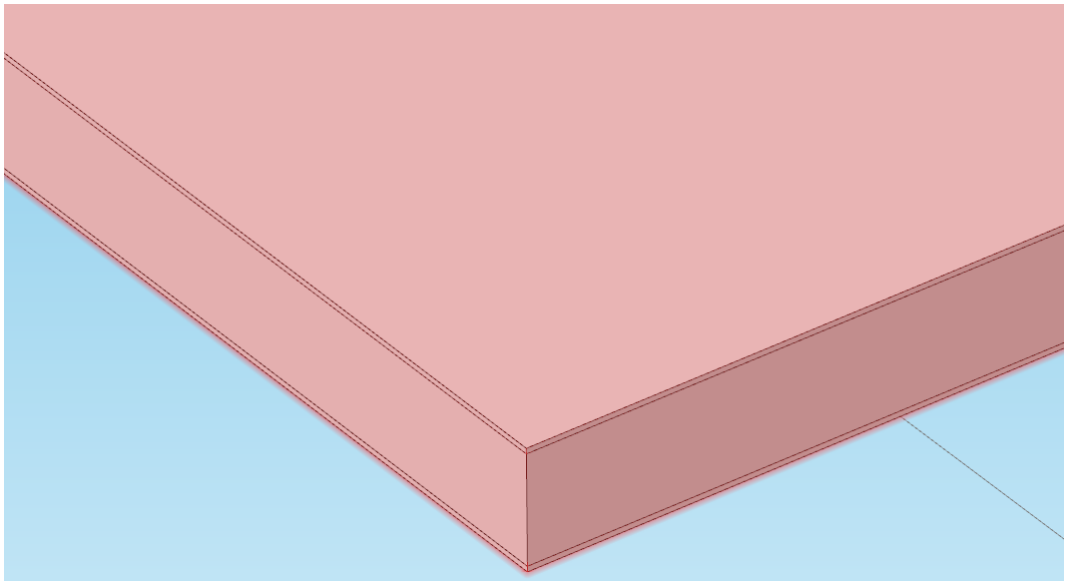

Figure 4.4: IPMC Strip Zoomed in

The final 2D geometry used for solving the ion transport model is illustrated below.

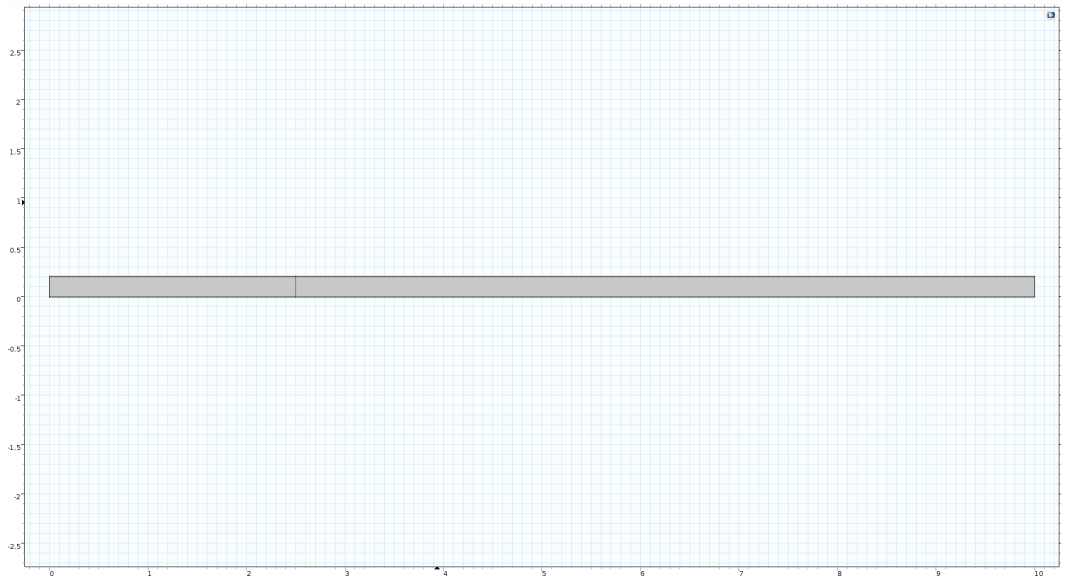

Figure 4.5: The Final 2D Geometry

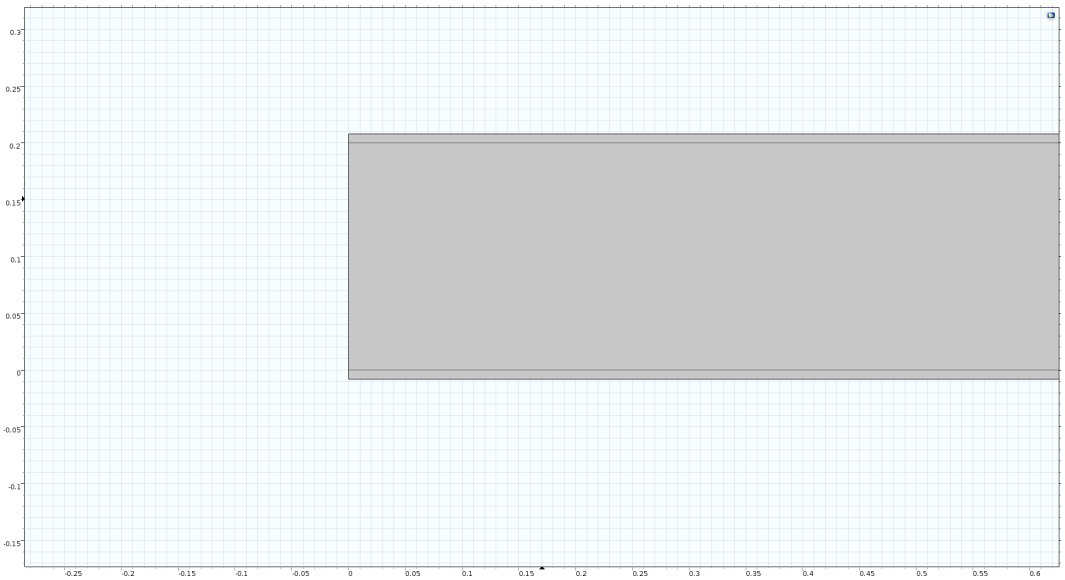

Figure 4.6: 2D Final Geometry zoomed in

The second geometry was constructing by attaching the IPMC strip onto the imported wing structure which was designed in Autodesk Inventor®. This geometry was constructed in order to solve the solid mechanics model. The finalized geometry is shown below.

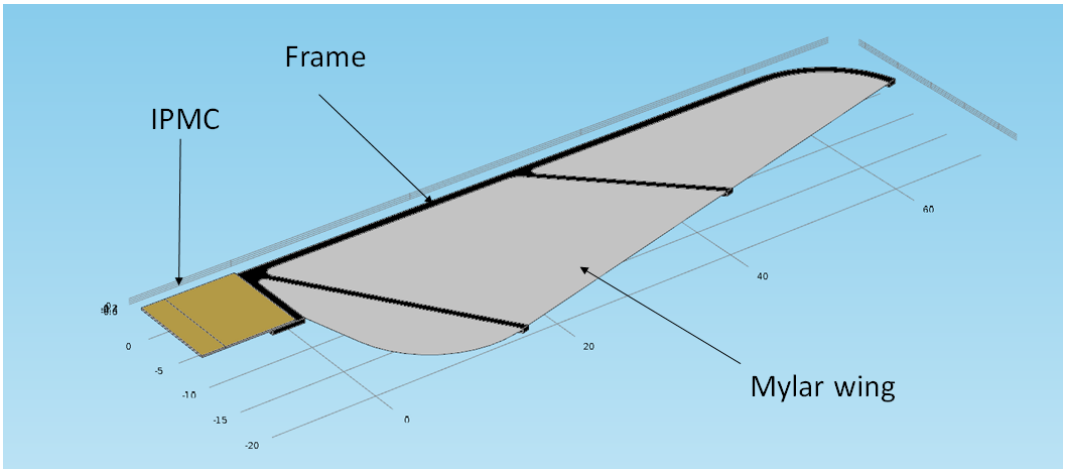

Figure 4.7: Finalized Wing Geometry for Mechanical Analysis

Values of dependent variables in the first geometry that needed to be used in the secon geometry were simply extruded using the 'genext' function available in Comsol Multiphysics®.

4.3.1.2 Meshing

Meshing for the ionic transport model was done very differently from the solid mechanics model. The mesh for the ionic transport model required very fine resolution along the z axis in the immediate vicinities of the electrodes as cation concentration varies very steeply in this region. On the other hand all the dependent variables in the ion transport model varied slightly in the x and y directions. Hence it was viable to generate elements with very high aspect ratios, which is necessary to avoid the very fine mesh resulting from the small dimensions of the electrodes. As you can see in following set of figures, the mesh is made up of prism shaped elements with very fine dimensions along the z-axis near the electrodes.

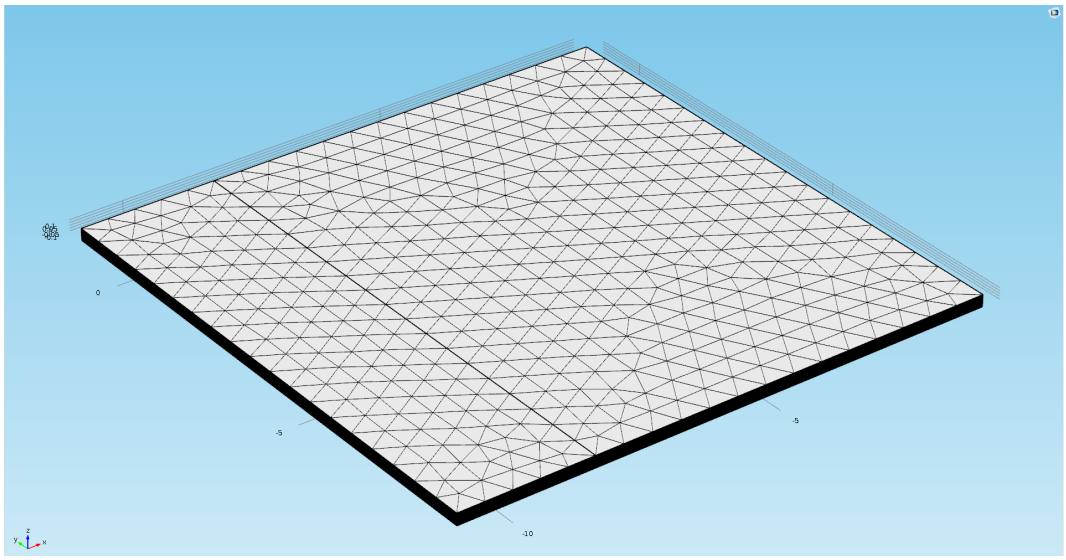

Figure 4.8: Mesh for Ionic Transport Model

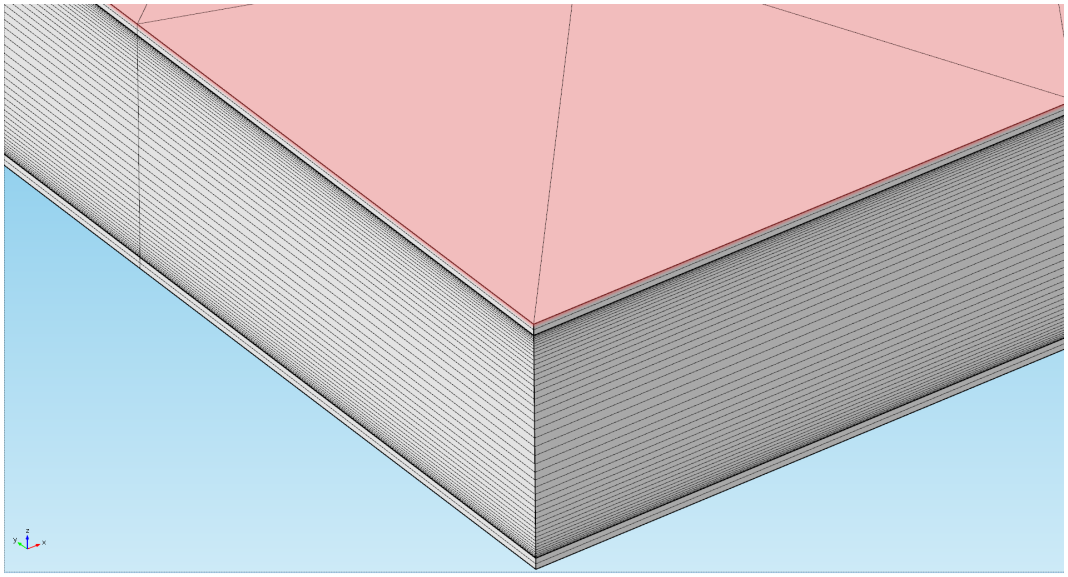

Figure 4.9: Mesh for Ionic Transport Mode - Closer Look

.

On analysing the 3D model it was found that the variables varied sharply along the z axis near the polymer electrode interface, and slightly along the z axis, with some relatively sharper changes near the clamp edge or electrical contact edge. On the other hand the variables remained almost unchanged along the Y-axis. Based on these observations an efficient mesh for analysing the 2D geometry was developed, which as illustrated in the figure below.

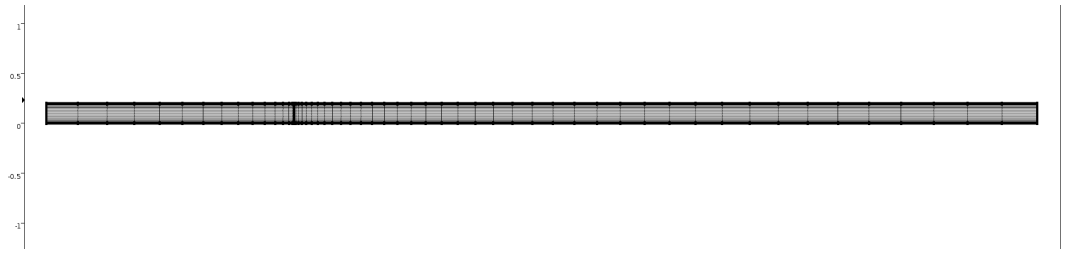

Figure 4.10: 2D Mesh

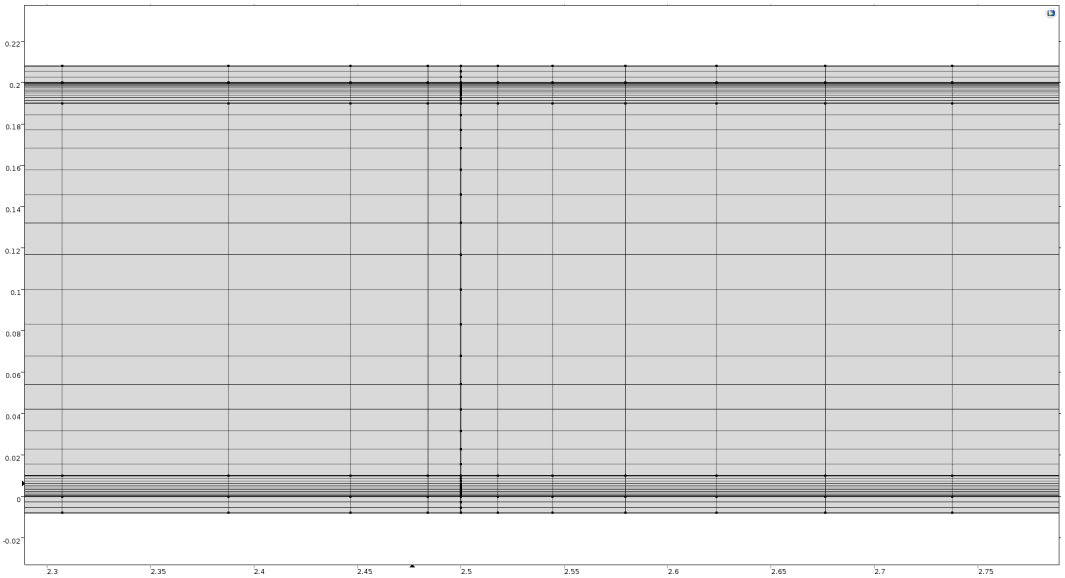

Figure 4.11: 2D mesh Zoomed in

Meshing for the solid mechanics model was generated using the default tetrahedral elements. This mesh was generated automatically in the software. The electrode layer on the IPMC and the Mylar film layer had to be excluded for the time being in order to avoid inconsistencies and to obtain a reasonable mesh. Further since these layers are very thin and as Aerodynamic interaction hasn't been included in the model, their contribution to the final results is negligible. The following figure shows the mesh used for the solid mechanics model.

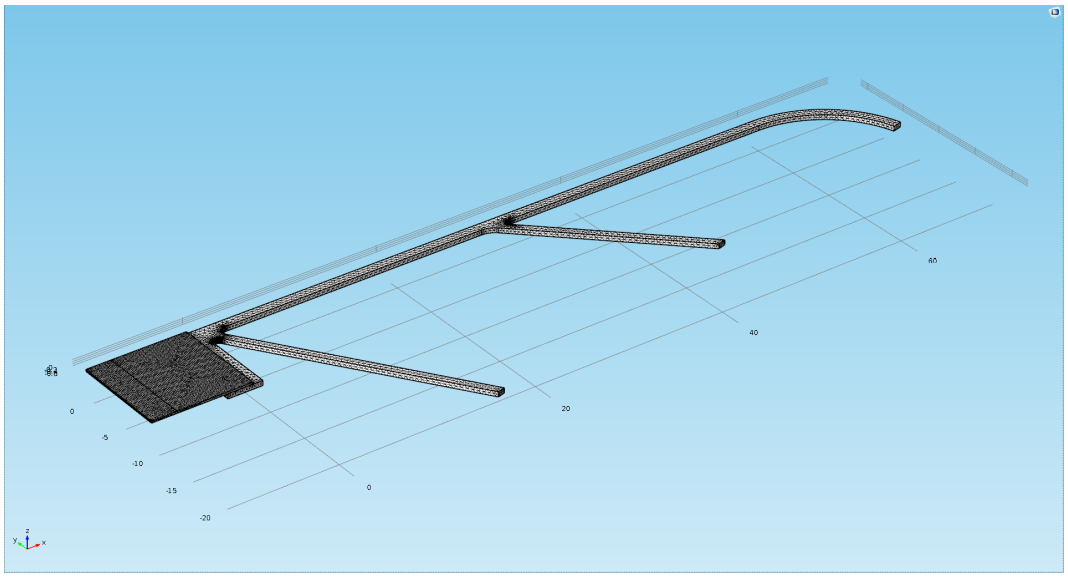

Figure 4.12: Mesh used for the Solid Mechanics Model

4.3.1.3 Physics

For the electro-mechanical transduction model the following Physics are used

1. The Electric Currents module (ec) for modeling the electrode layer and simulating the effect of electrode resistance.

2. The Chemical Transport Module (tds) which solves the Nernst Plank Equation for migration of ions due to electric fields.

$$\frac{\partial c}{\partial t} - \nabla.(D\nabla c + z\mu F c\nabla V) = 0$$

   The voltage gradient appearing in this equation is supplied by the following physics interface.

3. The General Form PDE (g) interface for solving the Poisson's equation to determine the internal potential gradient in the polymer.

$$-\nabla^2 V = \frac{\rho}{\varepsilon_o \varepsilon_r}$$

   Dirchlet Boundary conditions are applied at the electrode-polymer interface wherein the value for electric potential is supplied by the electric currents interface.

4. The Solid Mechanics Interface (solid) for solving the solid mechanics problem on the second geometry. A fixed constraint was imposed on the left end of the IPMC strip and force couplings were used to simulate the boundary loads acting on the polymer-electrode interface based on the cation concentration in the region.

4.3.2 Solver

1. For the first geometry and the ion transport model a Time Dependent study was carried out using an iterative solver (GMRES) in the 3D case. For the 2D model a fully coupled direct MUMPS solver was used. The time steps taken were equivalent to $(1/40)^{th}$ of the time period of the supplied sinusoidal voltage and the range of time steps covered 16 -20 whole cycles of the applied voltage.

2. For the solid mechanics model another independent Time Dependent study was carried out using a direct solver (MUMPS). The time steps taken were similar to the first study.

4.3.3 Post Processing

Many of the essential plots are automatically generated after a simulation is run in Comsol Multiphysics®. A few other plots relevant to our study were generated manually all of which are discussed in the next section.

Chapter 5

Results and Conclusion

5.1 Ionic Transport Model

In this section the distribution of potential and cations within the polymer membrane were observed and studied. The following plot shows the distribution of potential within the polymer membrane. The potential difference gradually decreases along the polymer towards the free end.

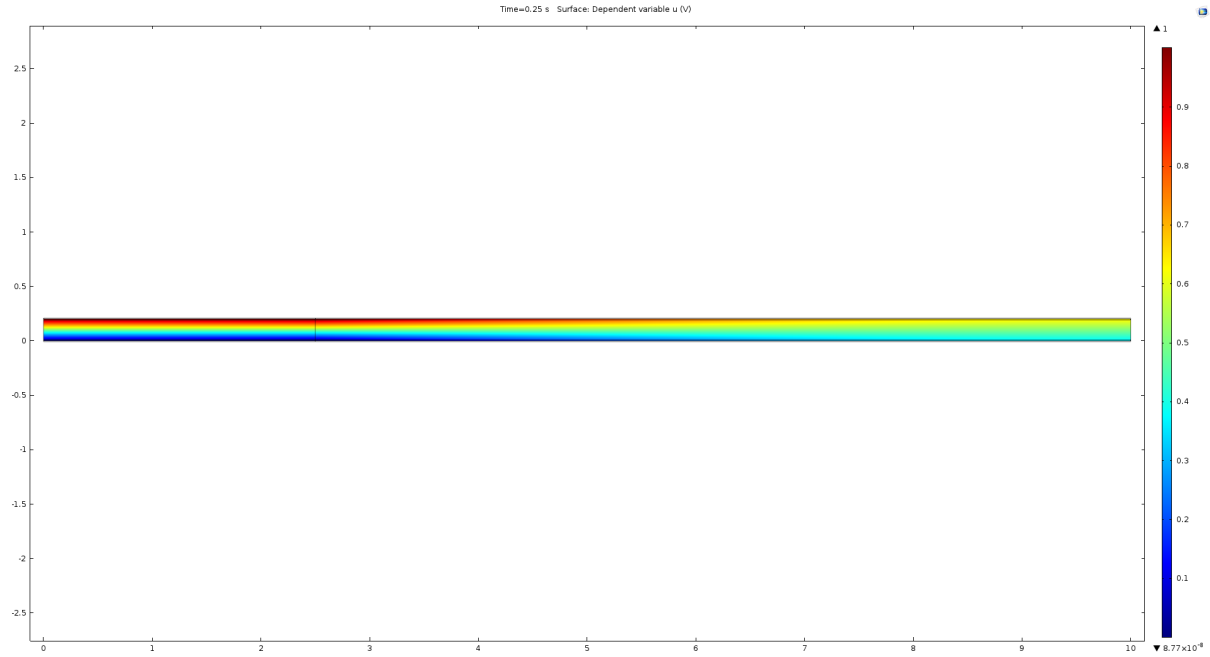

Figure 5.1: Voltage distribution within the membrane, ϕ

Similarly, the distribution of cations is depicted in the following plot

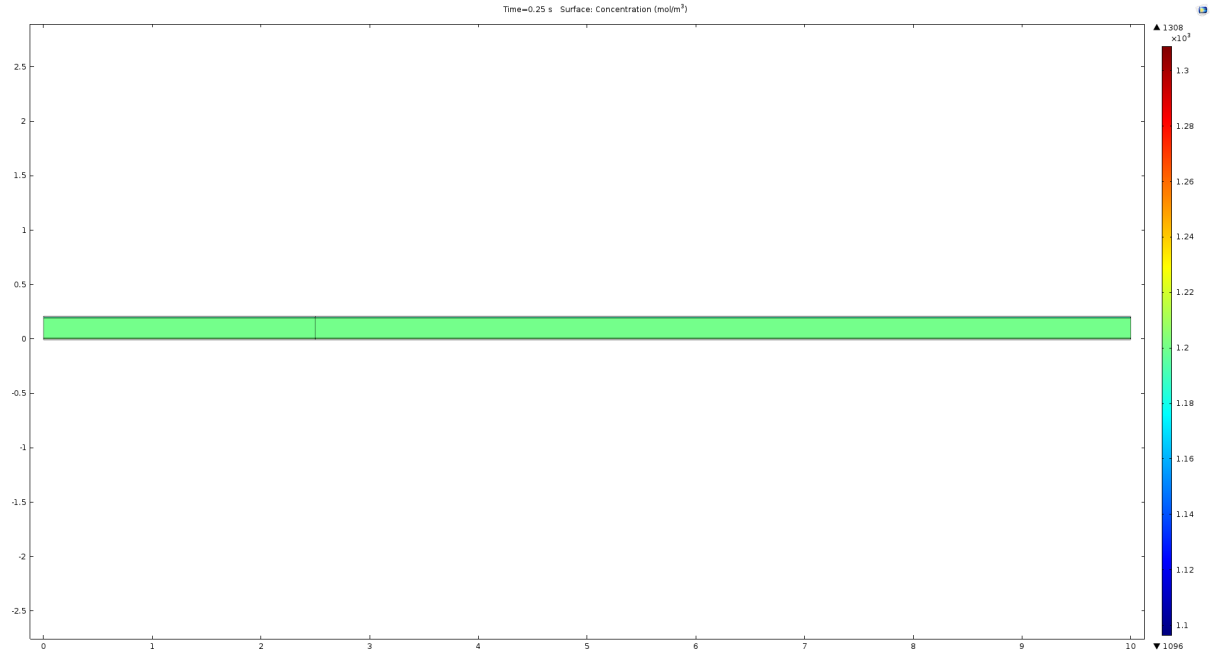

Figure 5.2: Cation Concentration within the polymer

It can be seen that the change in concentration is very sharp near the polymer-electrode interfaces and remain unchanged towards the centre. The following plots illustrate this behavior

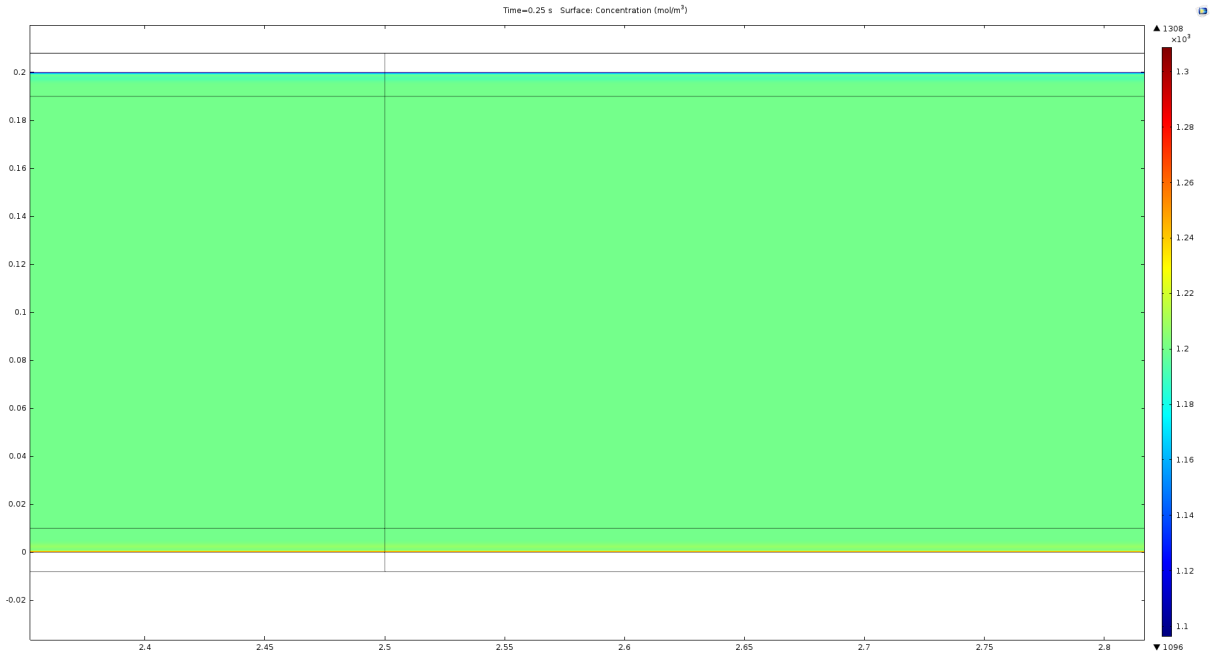

Figure 5.3: Cation concentration zoomed in

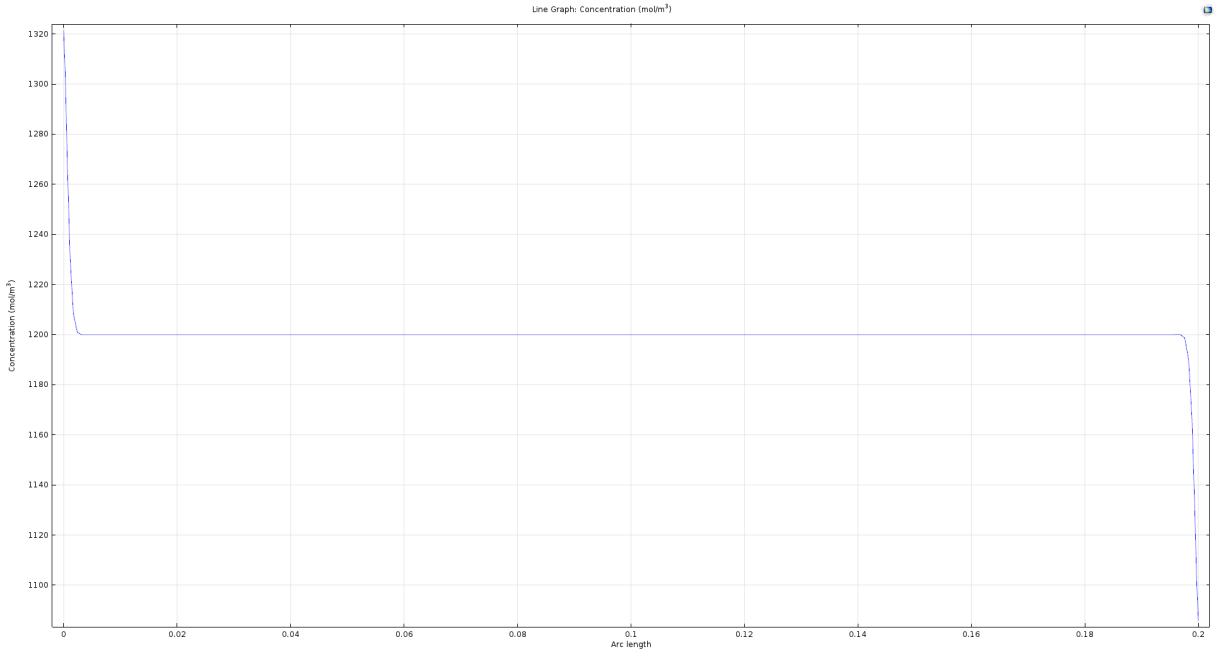

Figure 5.4: Cation concentration along the cross-section

The average cation concentration along the upper polymer boundary and the lower polymer boundaries of the IPMC strip were found to vary sinusoidally in tandem to the supplied sinusoidal voltage as input. A small phase lag in the response of the cations to the supplied voltage is also observed, which can be attributed to the finite velocity at which ions move within the polymer. The following plots illustrate the same for a 2mm thick IPMC strip subjected to a 1 Hz sinusoidal input voltage. (The horizontal line at 1200 $molm^{-3}$ depicts the initial cation concentration in the polymer)

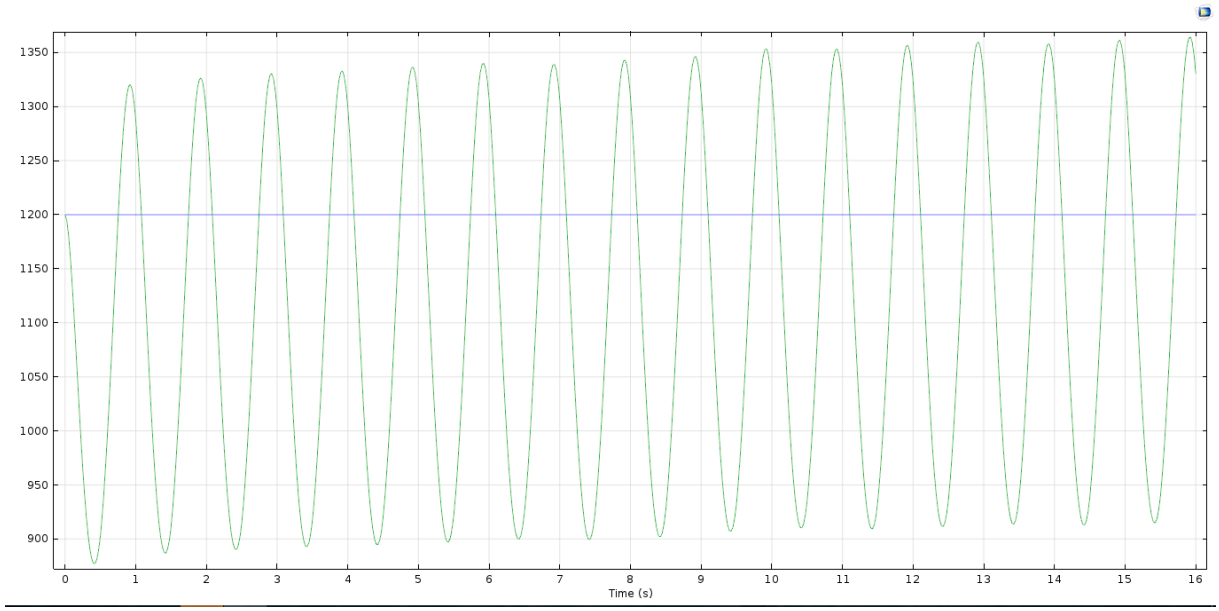

Figure 5.5: Average Cation Concentration at Upper Boundary

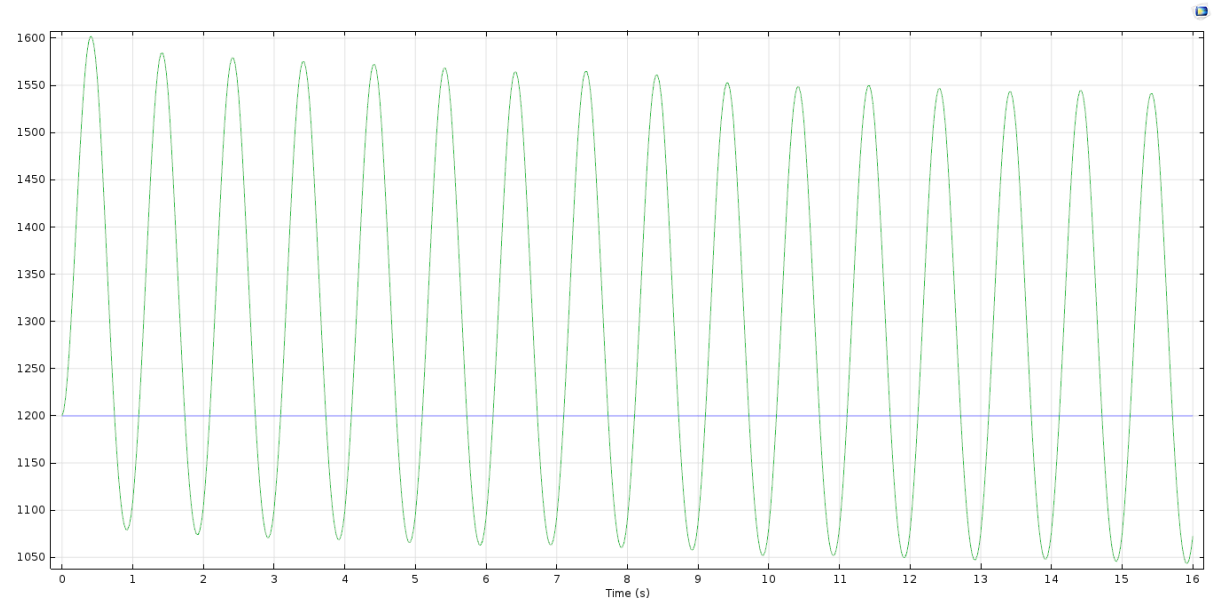

Figure 5.6: Average Cation Concentration at Lower Boundary

5.2 Solid Mechanics Model

During simulation of the wing in Comsol Multiphysics a clear flapping motion was observed for a 1 Hz sinusoidal voltage input. The following figures illustrate one flapping cycle starting at 6.1s after the start of the simulation.

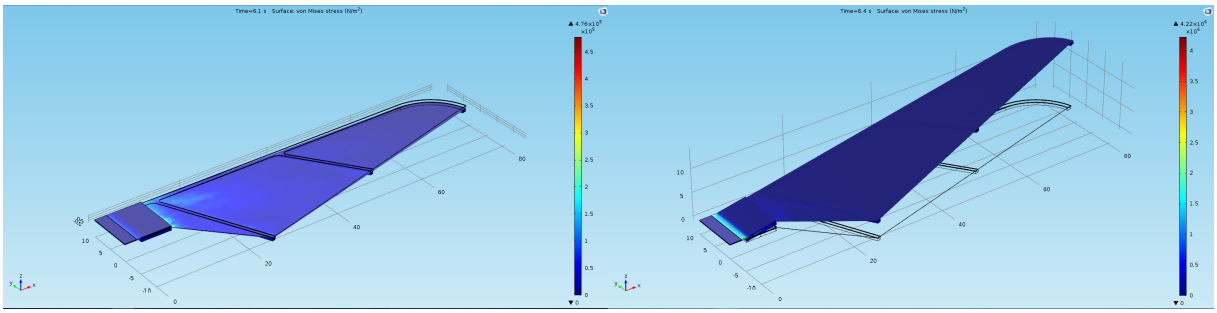

(a) Wing at 6.1s

(b) Wing at 6.4s

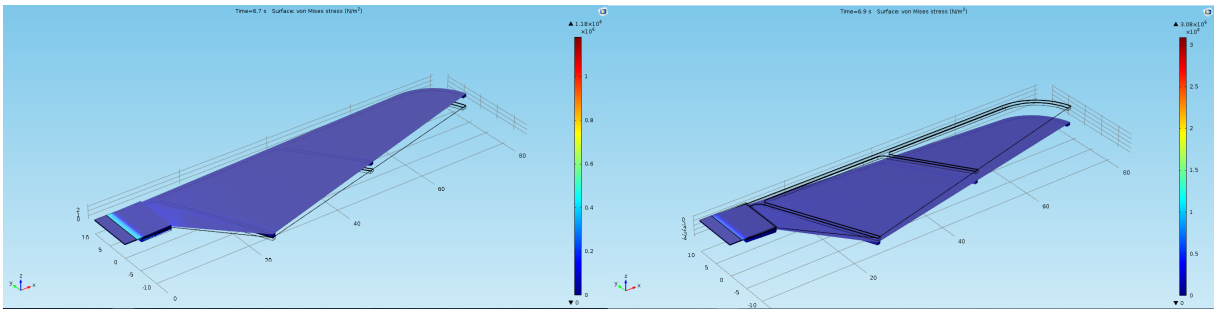

(c) Wing at 6.7s

(d) Wing at 6.9s

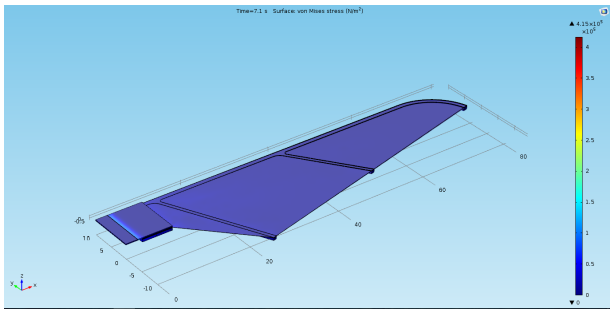

(e) Wing at 7.1s

Figure 5.7: Complete flapping cycle

The above plots also give us an insight on the stress distribution within the wing structure. It was observed that maximum stresses induced were either in the IPMC strip or in the epoxy adhesive layers. These were also the weakest materials making up the wing. Hence stress studies were only carried out on the IPMc strip and the two adhesive layers.

All these simulations were carried out for three degrees of overlap of the IPMC strip on the wing structure as shown in the images bellow.

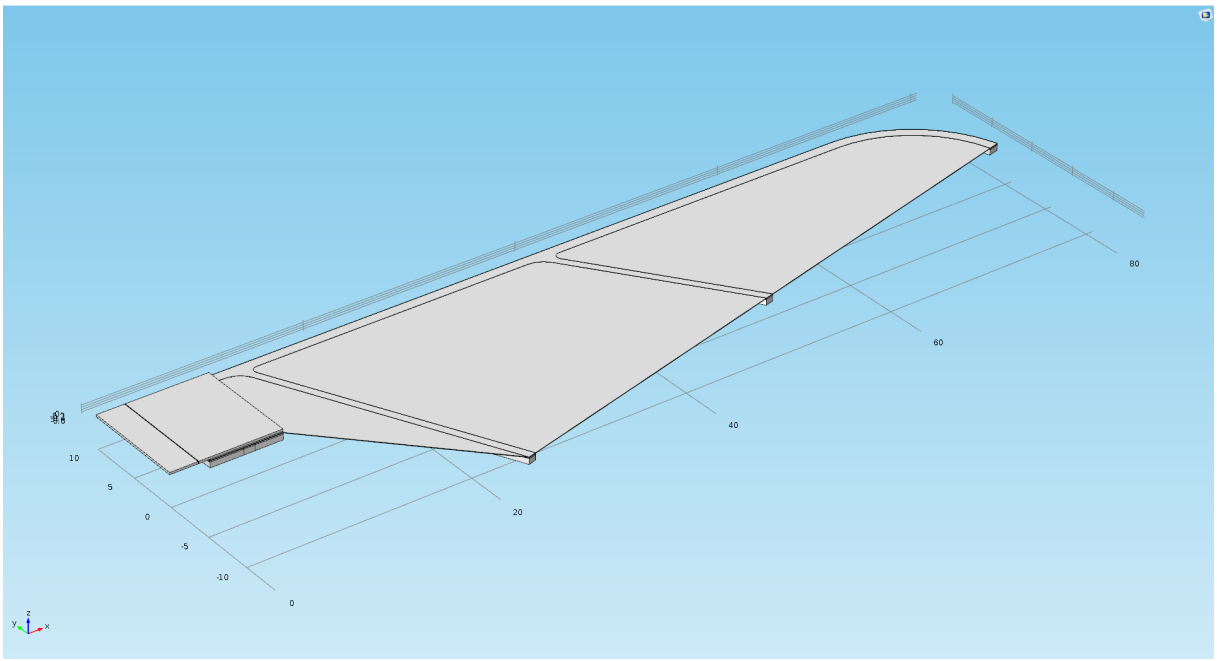

Figure 5.8: 6.5 mm Overlap

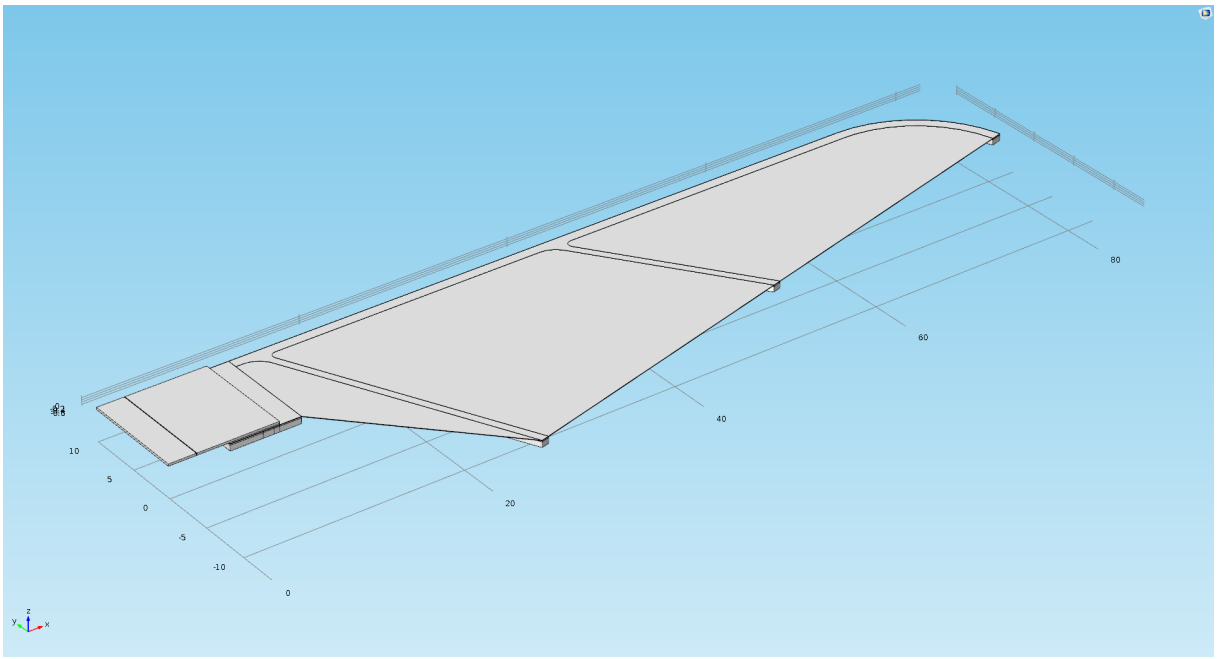

Figure 5.9: 4.5 mm Overlap

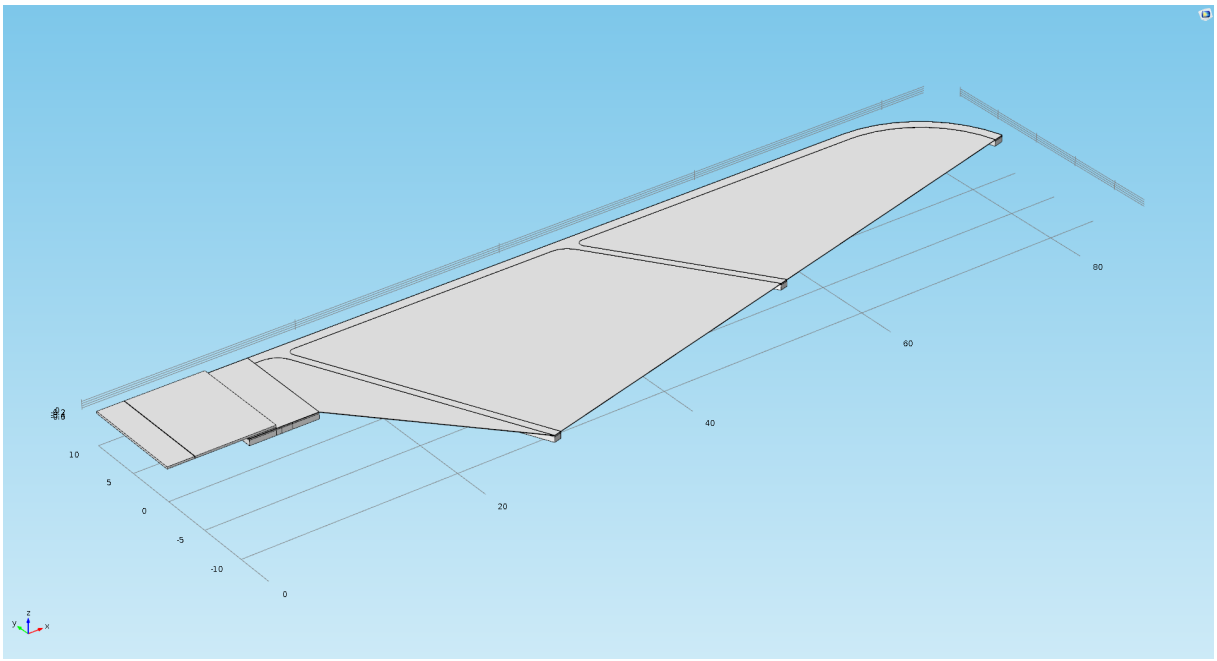

Figure 5.10: 2.5 mm Overlap

The wing tip deflection along the vertical for a 1 Hz sinusoidal voltage input for a wing actuated with a 2 mm thick IPMC were as follows.

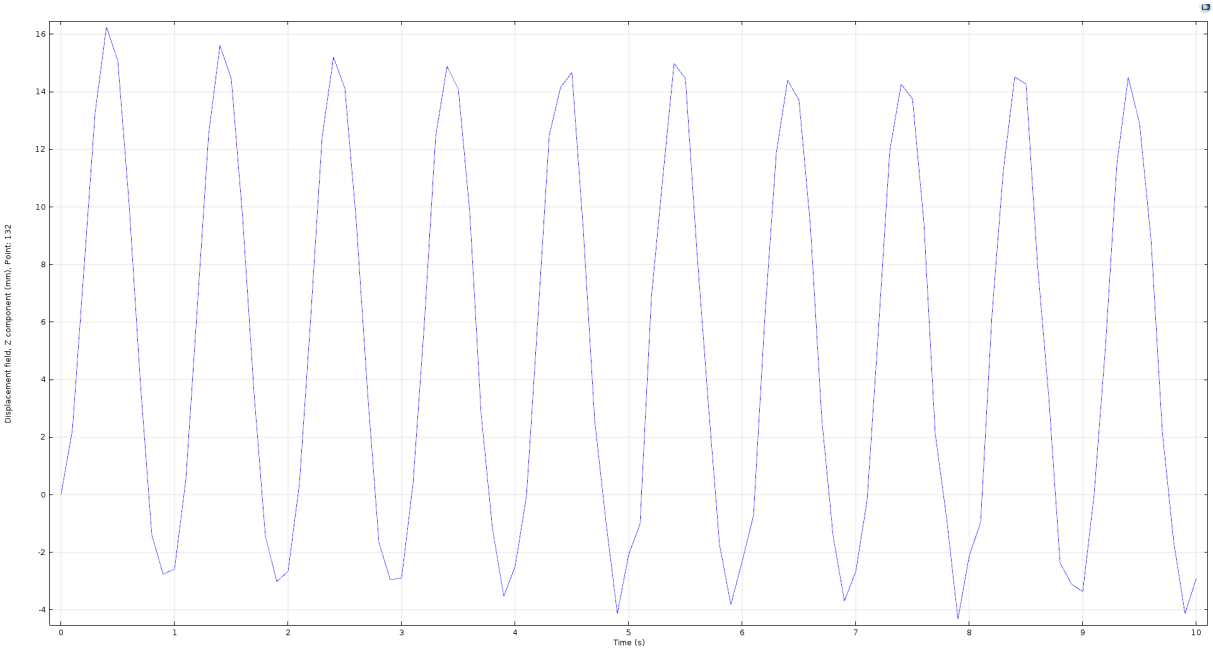

Figure 5.11: Wing Tip Displacement for 6.5 mm Overlap

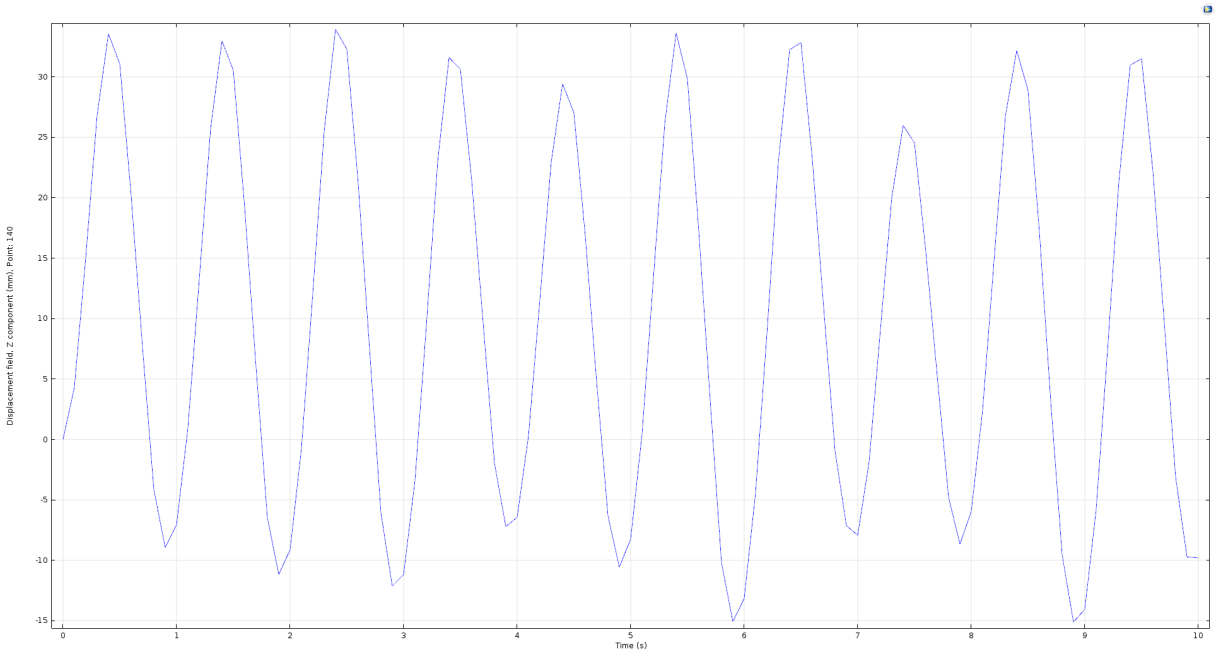

Figure 5.12: Wing Tip Displacement for 4.5 mm Overlap

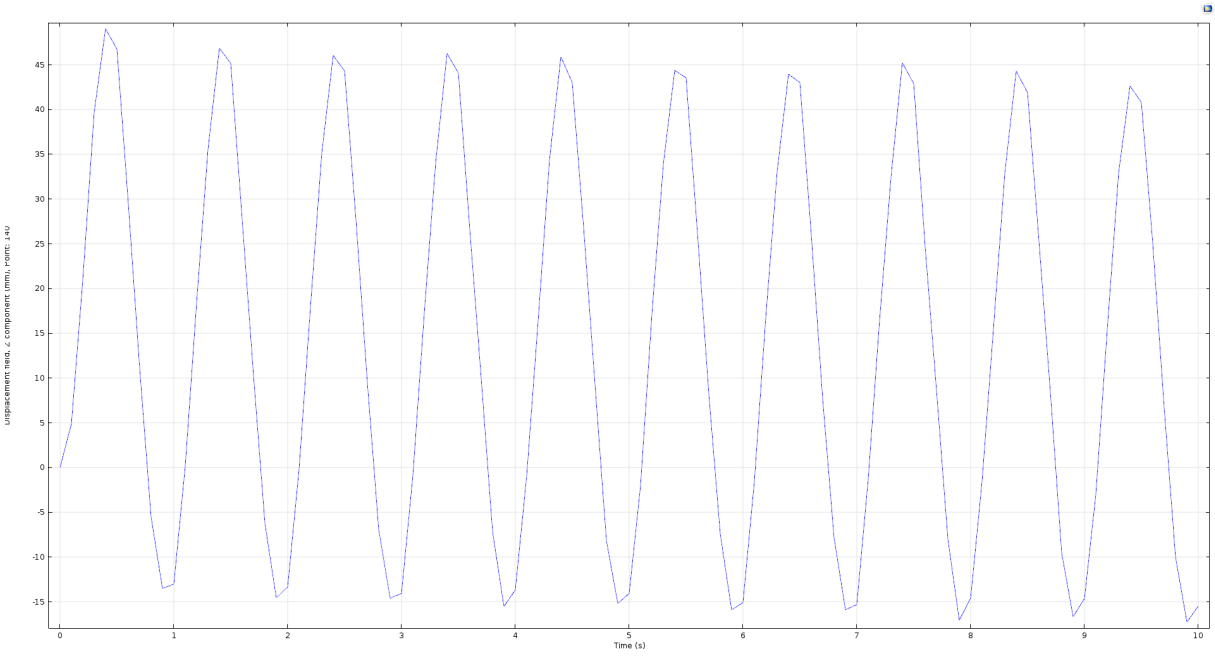

Figure 5.13: Wing Tip Displacement for 2.5 mm Overlap

From the above plots, it can be seen that flapping angle increases as the overlap decreases at 1 Hz input. The corresponding Von Mises Stresses in the IPMC strip and the epoxy adhesive layers used to bind the wing structure to the IPMC strip, respectively, are depicted in the plots shown below.

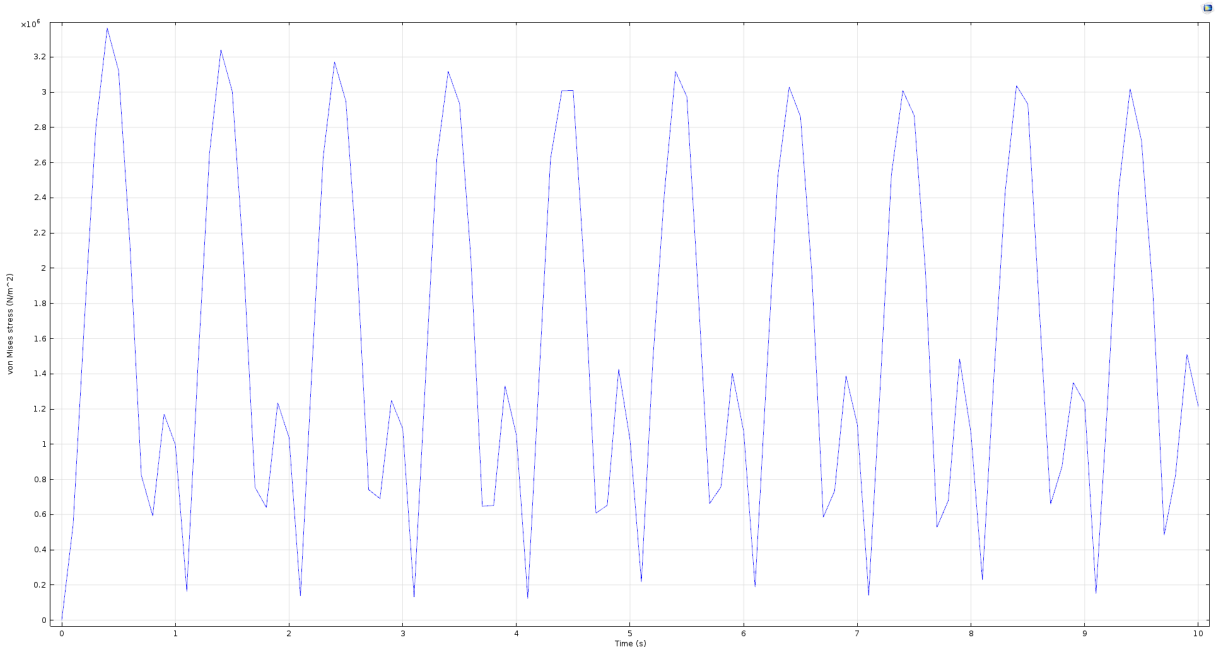

(a) IPMC

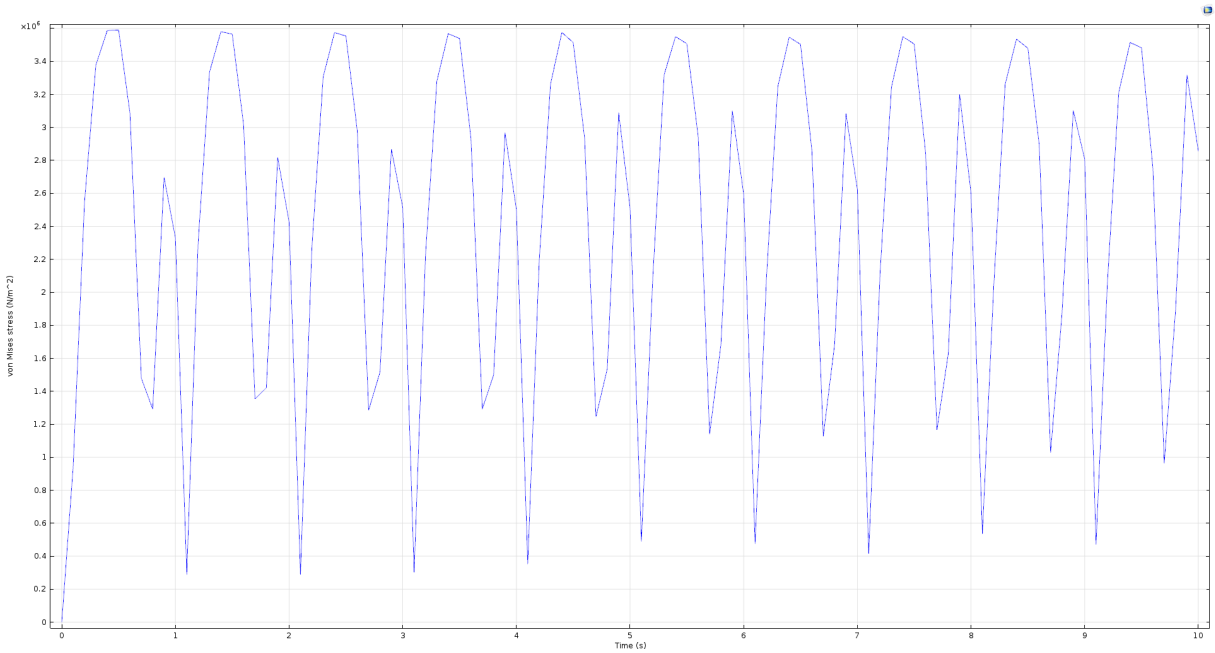

(b) Epoxy

Figure 5.14: Von Mises Stresses for 6.5 mm Overlap

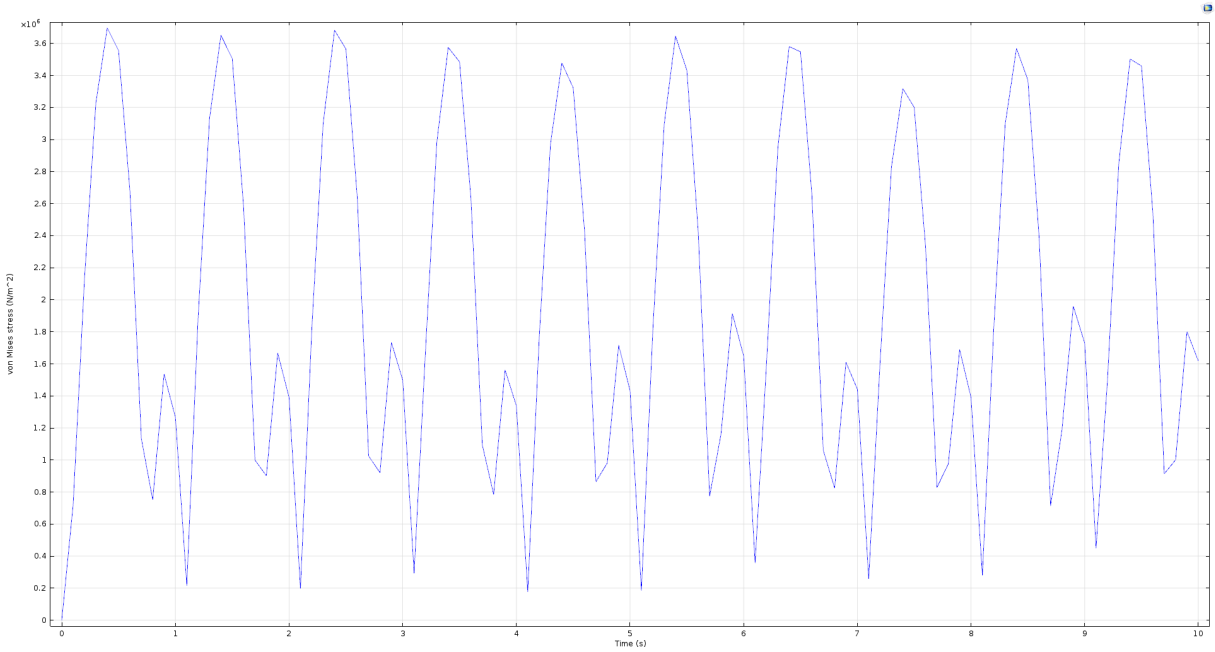

(a) IPMC

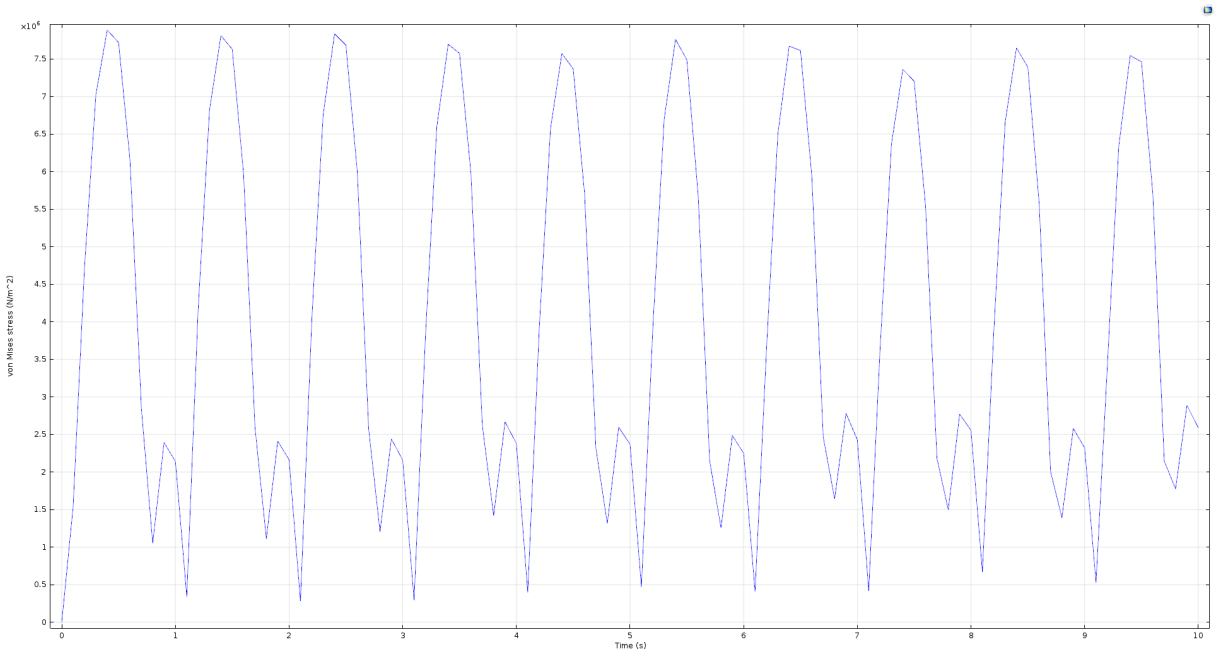

(b) Epoxy

Figure 5.15: Von Mises Stresses for 4.5 mm Overlap

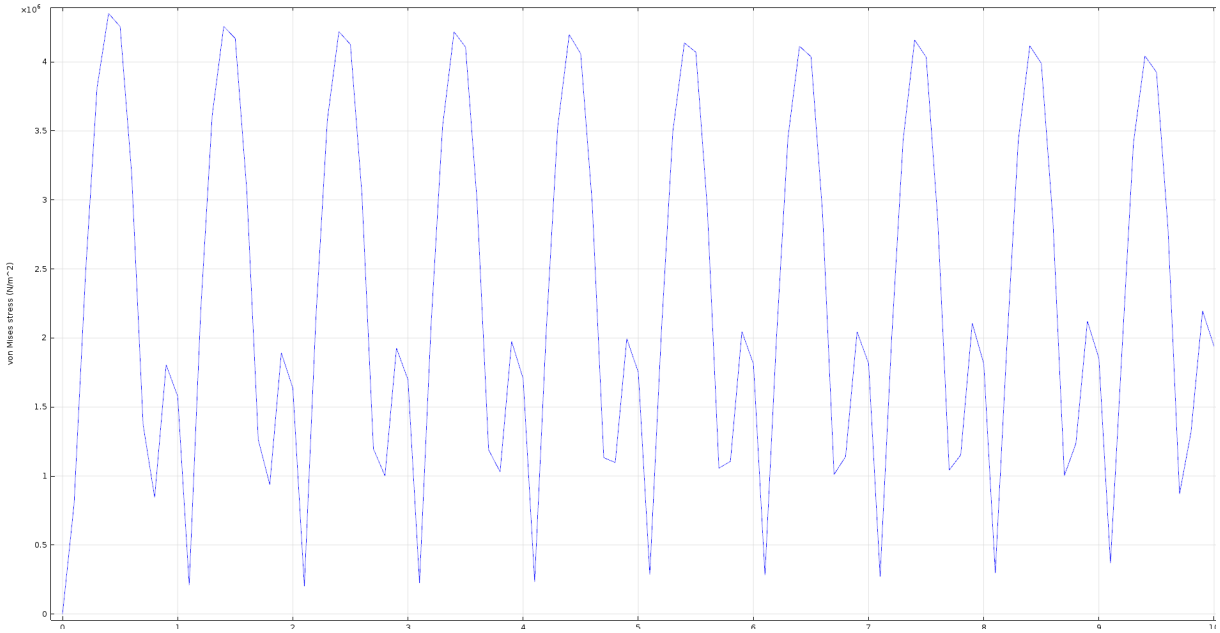

(a) IPMC

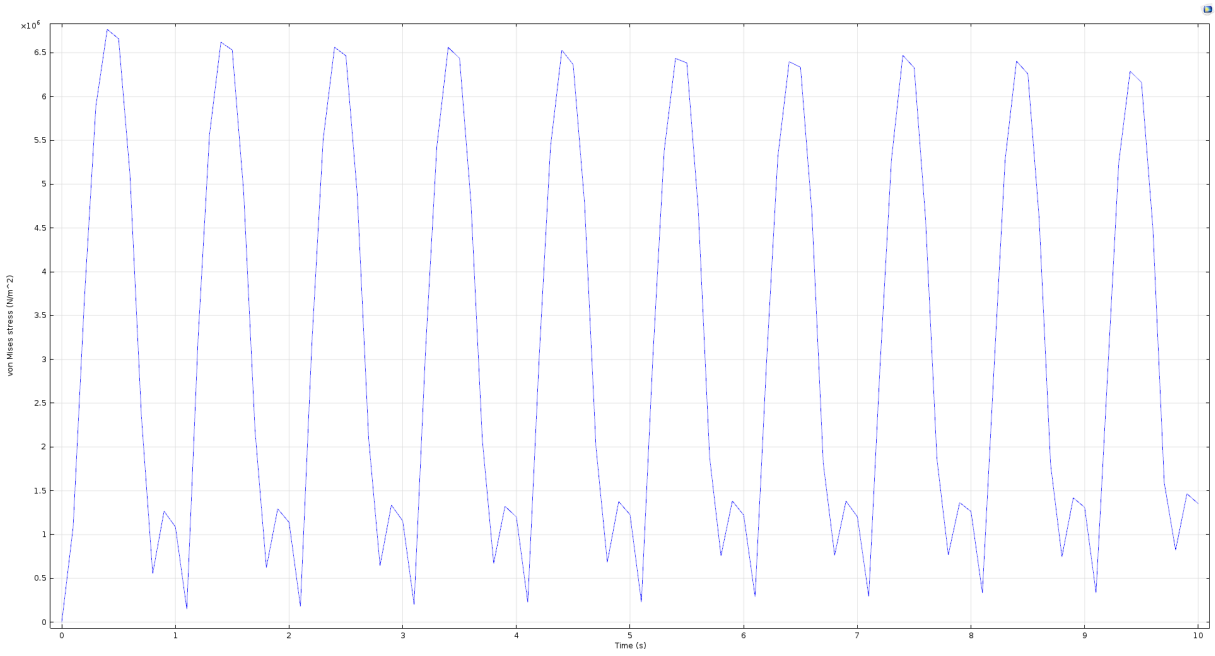

(b) Epoxy

Figure 5.16: Von Mises Stresses for 2.5 mm Overlap

These plots show that the maximum stress in the IPMC strip increases with the decrease in the area of overlap. But the maximum stress in the epoxy layer increases and then decreases. All these stresses are however within the safe loading limits for their respective materials.

Simulations were also carried out with 5 mm thickness IPMC strip. since maximum efficiency was found at 2.5 mm over lap and considering that the thicker IPMC is less flexible and can hence generate more actuation force the 2.5 mm overlap case seemed to be ideal. Hence the simulations in this case were all carried out at 2.5 mm overlap. The displacements

observed, however, were substantially lower than those with 2 mm thickness IPMC

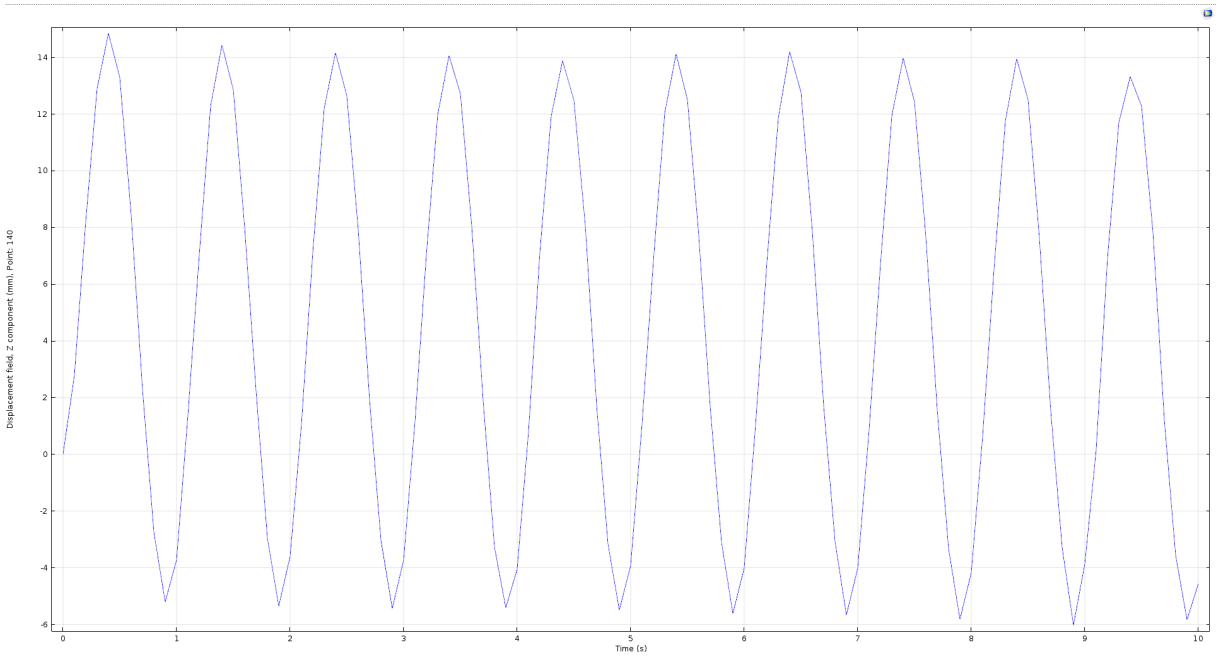

Figure 5.17: Wing Tip Displacement for 5mm thick IPMC and 2.5 mm Overlap

The corresponding stresses that were obtained were also much low compared to the previous case where a 2 mm thick IPMC was used as the actuator. The stress plots obtained were as follows.

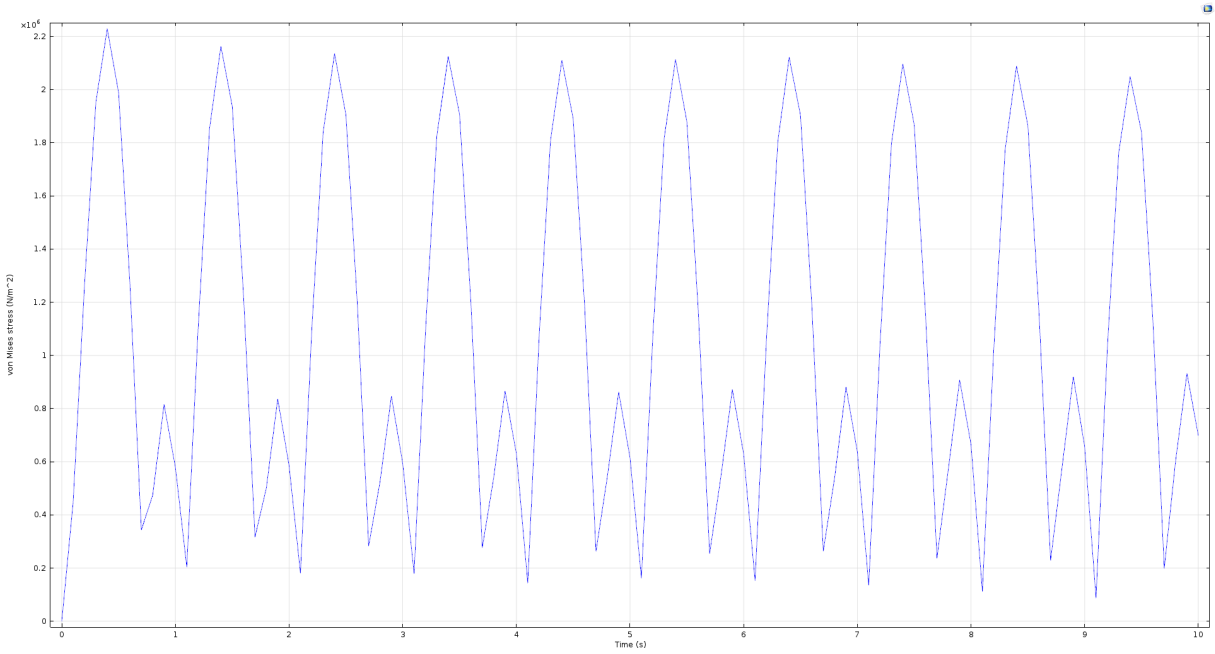

(a) IPMC

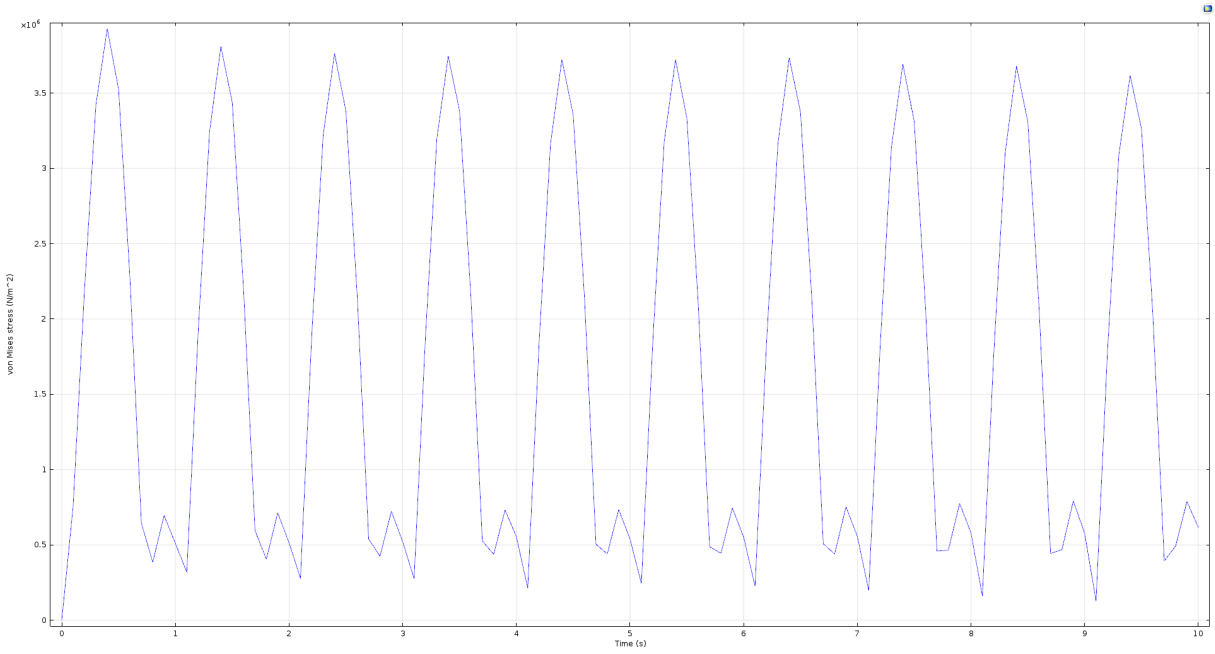

(b) Epoxy

Figure 5.18: Von Mises Stresses for 5mm thick IPMC and 2.5 mm Overlap

The same simulation was carried out at 5 Hz input for 2 mm thickness IPMC strip. The tip displacement obtained was quite less compared to that obtained using a 1 Hz input and the stresses generated were also considerably less. The tip displacements and the stresses

generated are illustrated in the following plots.

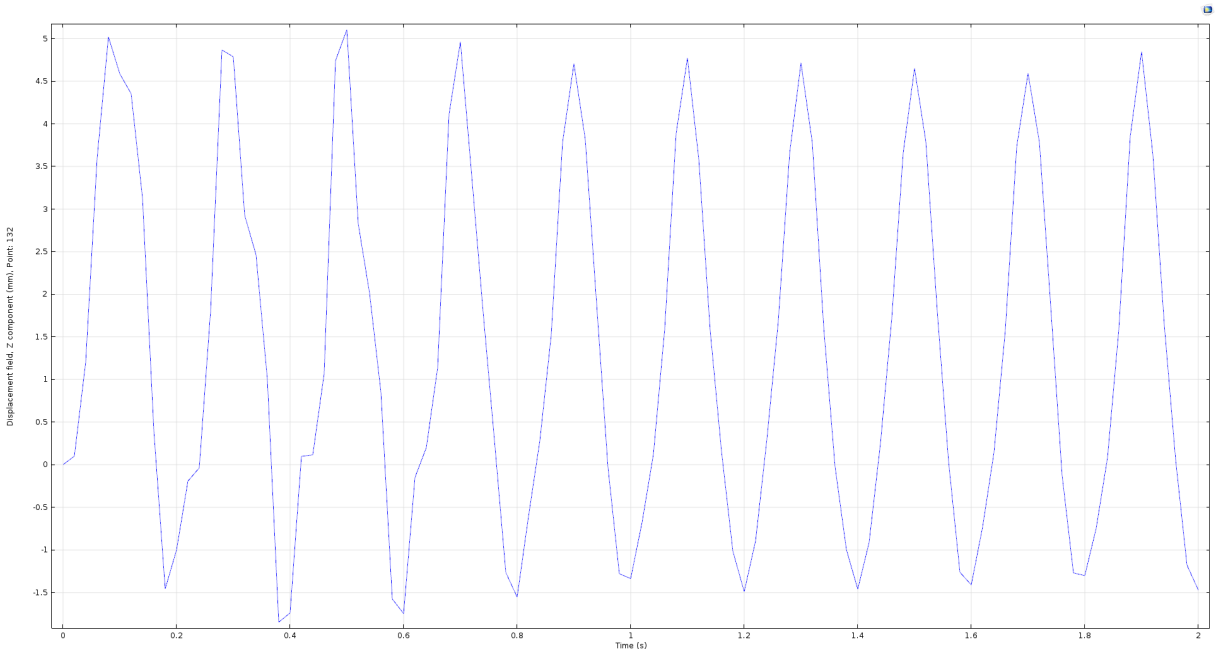

Figure 5.19: Tip Displacement for 5 Hz Input and 6.5mm overlap

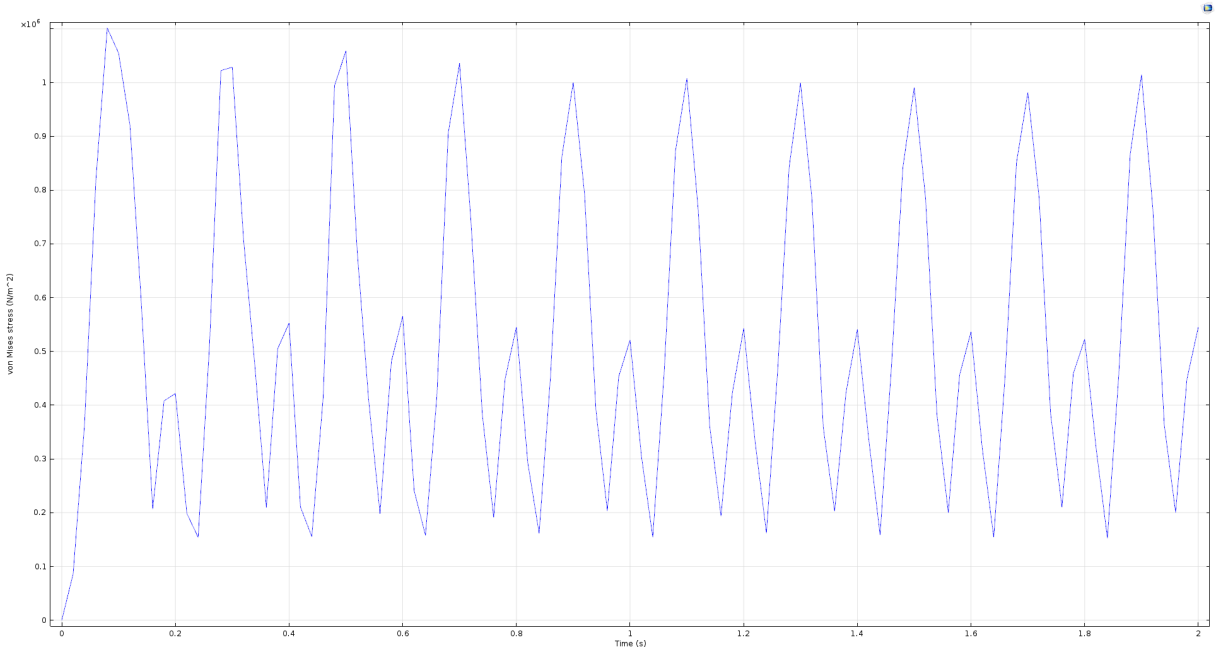

(a) IPMC

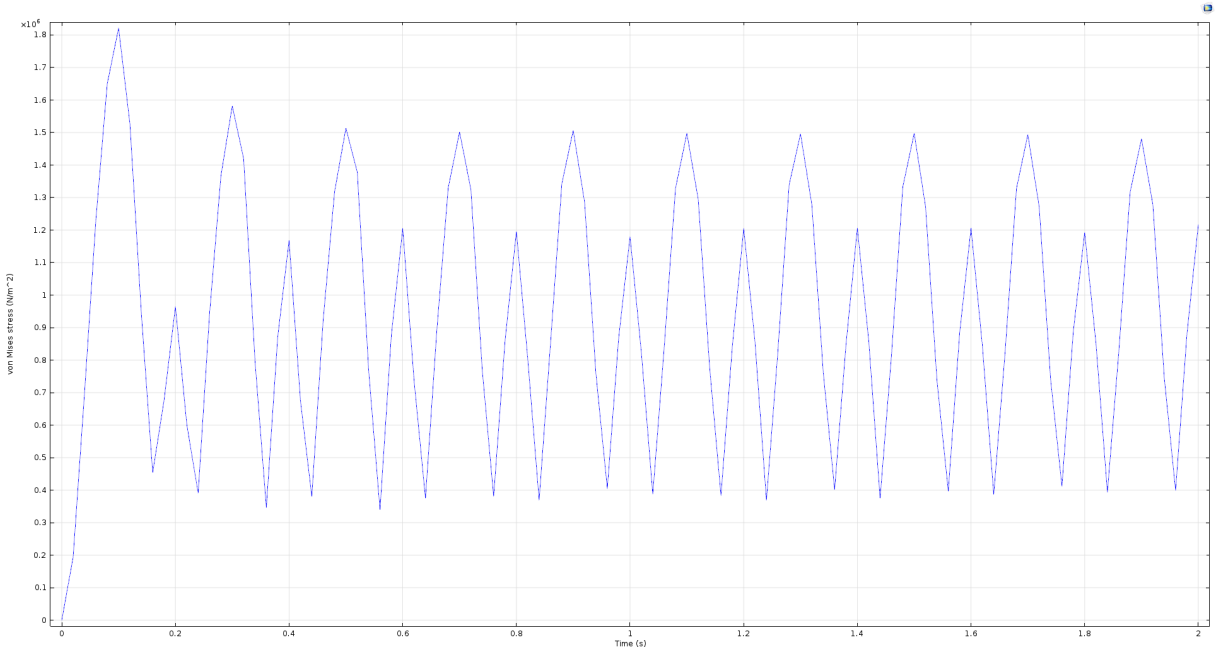

(b) Epoxy

Figure 5.20: Von Mises Stresses for 5 Hz input and 6.5 mm overlap

It was observed that for lower values of overlap, the flapping motion turned inconsistent. This can be attributed to the soft nature of IPMc and hence the limited actuation force which fails to keep up with the inertial load during fast flapping.

5.3 Discussions/Conclusions

1. As observed from the results obtained IPMCs are indeed viable as actuators for flapping wing fliers.

2. The flapping angles obtained at 1 Hz are quite high and might be sufficient for successful flight. We also found that for both 2 mm and 5 mm thick IPMC actuators, the maximum tip displacements and hence the maximum flapping angle could be obtained at least overlap (2.5 mm) of the IPMC on the wing structure.

3. Further, by inspecting the maximum Von Mises stresses developed within the structure, the design was found to be safe. But at the same time higher stresses were generated within the materials in these cases. This also exposed a limitation of IPMCs to generate enough force and hence a suitable flapping motion at higher frequencies in our current design. This also suggests that IPMCs might be more attractive when looking at much smaller scales for MAV or wing design, where the inertial loading of the wing can substantially less.

4. A wing design which is much more light and strong can also be a possible solution, although the current design is quite light, weighing just around 0.26 g. Other ways in which these problems can be circumvented through is by choosing a careful design and suitable mechanism, using gears or bar linkages, to enhance the flapping motion.

Chapter 6

Scope for Future Work

- Improving the functional properties of IPMC through improvising the techniques of manufacture and optimizing the composition of the material.
- Optimizing the design of flapping wings and the materials used to achieve the following - 1. Optimal first natural frequency; 2. Lower added mass effect and lower inertial drag on the wings; 3. Increased surface area to obtain optimal wing loading.
- Developing novel configurations to enable bending as well as twisting motion of the wings.
- Developing and testing more flapping profiles.
- Reliability studies on flapping wing MAV wings manufactured with IPMCs, involving, fracture and damage mechanics, fatigue analysis, etc.

Bibliography

[1] Barbar Jawad Akle. *Characterization and Modeling of the Ionomer-Conductor Interface in Ionic Polymer Transducers*. PhD thesis, Virginia Polytechnic Institute and State University, Blacksburg, Virginia, 07 2005.

[2] Michael L Anderson. *Design and Control of Flapping Wing Micro Air Vehicles*. PhD thesis, AIR FORCE INSTITUTE OF TECHNOLOGY, 09 2011.

[3] M D Bennett and D J Leo. Manufacture and characterization of ionic polymer transducers employing non-precious metal electrodes. *Smart Materials and Structures*, 12(3):424, 2003.

[4] Zheng Chen, Stephan Shatara, and Xiaobo Tan. Modeling of biomimetic robotic fish propelled by an ionic polymer–metal composite caudal fin. *IEEE/ASME transactions on mechatronics*, 15(3):448–459, 2010.

[5] C.K. Chung, P.K. Fung, Y.Z. Hong, M.S. Ju, C.C.K. Lin, and T.C. Wu. A novel fabrication of ionic polymer-metal composites (ipmc) actuator with silver nano-powders. *Sensors and Actuators B: Chemical*, 117(2):367 – 375, 2006. The 13th International Conference on Solid-State Sensors, Actuators and Microsystems.

[6] A. Eisenberg and J. S. Kim. *Polymeric materials encyclopedia*, chapter Ionomers (Overview), pages 3435–3454. Number v. 2 in Polymeric Materials Encyclopedia. CRC Press, 1996.

[7] Shridhar P. Gejji, C. H. Suresh, Libero J. Bartolotti, and Shridhar R. Gadre. Electrostatic potential as a harbinger of cation coordination:â cf3so3- ion as a model example. *The Journal of Physical Chemistry A*, 101(31):5678–5686, 1997.

[8] P. J. James, J. A. Elliott, T. J. McMaster, J. M. Newton, A. M. S. Elliott, S. Hanna, and M. J. Miles. Hydration of nafion® studied by afm and x-ray scattering. *Journal of Materials Science*, 35(20):5111–5119, 2000.

[9] Byungkyu Kim, Byung M. Kim, Jaewook Ryu, In-Hwan Oh, Seung-Ki Lee, Seung-Eun Cha, and Jungho Pak. Analysis of mechanical characteristics of the ionic polymer metal composite (ipmc) actuator using cast ion-exchange film, 2003.

[10] Hong-Il Kim, Dae-Kwan Kim, and Jae-Hung Han. Study of flapping actuator modules using ipmc, 2007.

[11] Kwang J. Kim and Mohsen Shahinpoor. A novel method of manufacturing three-dimensional ionic polymerâmetal composites (ipmcs) biomimetic sensors, actuators and artificial muscles. *Polymer*, 43(3):797 – 802, 2002. Mattice Special Issue.

[12] Sang-Mun Kim and Kwang J Kim. Palladium buffer-layered high performance ionic polymerâmetal composites. *Smart Materials and Structures*, 17(3):035011, 2008.

[13] Ahn Kyoung Kwan and Doan Ngoc Chi Nam. *Smart Actuation and Sensing Systems - Recent Advances and Future Challenges*. InTech, 10 2012.

[14] S Lee, H Park, Surya D Pandita, and Youngtai Yoo. Performance improvement of ipmc (ionic polymer metal composites) for a flapping actuator. *International Journal of Control Automation and Systems*, 4(6):748, 2006.

[15] P. Millet, F. Andolfatto, and R. Durand. Preparation of solid polymer electrolyte composites: investigation of the precipitation process. *Journal of Applied Electrochemistry*, 25(3):233–239, 1995.

[16] P. Millet, M. Pineri, and R. Durand. New solid polymer electrolyte composites for water electrolysis. *Journal of Applied Electrochemistry*, 19(2):162–166, 1989.

[17] Sia Nemat-Nasser. Micromechanics of actuation of ionic polymer-metal composites. *Journal of Applied Physics*, 92(5):2899–2915, 2002.

[18] Sia Nemat-Nasser and Jiang Yu Li. Electromechanical response of ionic polymer-metal composites. *Journal of Applied Physics*, 87(7):3321–3331, 2000.

[19] Sia Nemat-Nasser and Chris W Thomas. *Electroactive Polymer (EAP) Actuators as Artificial Muscles: Reality, Potential and Challenges*, volume PM136, chapter 6 - "Ionomeric Polymer-Metal Composites", pages 171 – 230. SPIE PRESS, 2004.

[20] K Oguro, Y Kawami, and H Takenaka. Bending of an ion-conducting polymer film-electrode composite by an electric stimulus at low voltage. *J. Micromachine*, 5:27–30, 1992.

[21] Viljar Palmre, David Pugal, Kwang J Kim, Kam K Leang, Kinji Asaka, and Alvo Aabloo. Nanothorn electrodes for ionic polymer-metal composite artificial muscles. *Scientific Reports*, 4:6176, Aug 2014. Article.

[22] Viljar Palmre, David Pugal, Kwang J Kim, Kam K Leang, Kinji Asaka, and Alvo Aabloo. Nanothorn electrodes for ionic polymer-metal composite artificial muscles. *Scientific Reports*, 4:6176, Aug 2014. Article.

[23] David Pugal. *Physics Based Model of Ionic Polymer-Metal Composite Electromechanical and Mechanoelectrical Transduction*. PhD thesis, University of Nevada, Reno, 08 2012.

[24] Tiwari R. Modeling and characterization of ipmc energy harvesters. *Saarbrucken: Lambert Academic*, 2010.

[25] E. J. Roche, M. Pineri, R. Duplessix, and A. M. Levelut. Small-angle scattering studies of nafion membranes. *Journal of Polymer Science: Polymer Physics Edition*, 19(1):1–11, 1981.

[26] M Shahinpoor. Conceptual design, kinematics and dynamics of swimming robotic structures using ionic polymeric gel muscles. *Smart Materials and Structures*, 1(1):91, 1992.

[27] Mohsen Shahinpoor and Kwang J Kim. The effect of surface-electrode resistance on the performance of ionic polymer-metal composite (ipmc) artificial muscles. *Smart Materials and Structures*, 9(4):543, 2000.

[28] H. Takenaka, E. Torikai, Y. Kawami, and N. Wakabayashi. Solid polymer electrolyte water electrolysis. *International Journal of Hydrogen Energy*, 7(5):397 – 403, 1982.

[29] R Tiwari and E Garcia. The state of understanding of ionic polymer metal composite architecture: a review. *Smart Materials and Structures*, 20(8):083001, 2011.

[30] R Tiwari and K J Kim. Disc-shaped ionic polymer metal composites for use in mechano-electrical applications. *Smart Materials and Structures*, 19(6):065016, 2010.

[31] T. Xue, R.B. Longwell, and K. Osseo-Asare. Mass transfer in nation membrane systems: Effects of ionic size and charge on selectivity. *Journal of Membrane Science*, 58(2):175 – 189, 1991.

[32] T. Xue, J.S. Trent, and K. Osseo-Asare. Characterization of nafion® membranes by transmission electron microscopy. *Journal of Membrane Science*, 45(3):261 – 271, 1989.

[33] Sung-Weon Yeom and Il-Kwon Oh. A biomimetic jellyfish robot based on ionic polymer metal composite actuators. *Smart Materials and Structures*, 18(8):085002, 2009.